npj | microgravity

Article

Published in cooperation with the Biodesign Institute at Arizona State University, with the support of NASA

https://doi.org/10.1038/s41526-025-00514-8

Abdominal LIPUS ameliorates simulated microgravity induced skeletal muscle atrophy via the gut-muscle axis

Yanan Yu[1], Yumei Zheng[1], Huiyuan Zhang[1], Xiushan Fan[1], Jianzhong Guo[2], Lijun Sun[1] ✉, Liang Tang[1] ✉ & Dean Ta[3,4] ✉

Study investigated if abdominal low-intensity pulsed ultrasound (LIPUS) alleviates simulated microgravity (hindlimb unloading, HU)-induced skeletal muscle atrophy by restoring gut microbiota. Mice were divided into control (NC), HU, and HU with daily abdominal LIPUS (HU + LIPUS) groups. Fecal microbiota transplantation (FMT) from LIPUS-treated mice to HU mice was also performed. After 28 days, abdominal LIPUS partially reversed HU-induced gut dysbiosis, restored intestinal barrier integrity, and increased short-chain fatty acid (SCFAs) levels. LIPUS downregulated muscle atrophy genes (MSTN, ActRIIB) and upregulated growth genes (Akt, mTOR) in HU mice, preventing muscle loss. SCFAs levels positively correlated with muscle function. HU mice receiving FMT from LIPUS-treated donors showed similar gut and muscle improvements as direct LIPUS treatment. Results demonstrate abdominal LIPUS ameliorates muscle atrophy by modulating the gut-muscle axis, offering a potential non-invasive strategy for astronauts and patients.

During prolonged space missions, astronauts confront the dual challenges of muscle atrophy and imbalance of gut microbiota. The human intestine is inhabited by an astonishing 100 trillion bacteria, collectively known as the gut microbiota. These bacteria form a rich and diverse community that coexists harmoniously with the host and plays a pivotal role in maintaining human health[1]. Prolonged exposure to weightlessness, however, can disrupt this microbial balance, leading to microbial dysbiosis. Changes in bacterial physiology under such conditions may profoundly impact the health and well-being of astronauts[2]. Previous research has demonstrated that microgravity influences bacteria in various ways, including their growth patterns, antibiotic resistance, and virulence[3]. Moreover, weightlessness has a detrimental effect on skeletal muscles, causing a reduction in muscle mass, strength, and endurance[4]. For instance, astronauts exposed to microgravity may experience a decline of up to 20% in average skeletal muscle mass and up to 30% in average skeletal muscle strength within just one month[5]. During a 12-day period of microgravity exposure, there can be a 10–30% decrease in muscle fiber cross-sectional area[6]. In summary, microgravity not only disrupts the balance of the gut microbiota but also leads to skeletal muscle atrophy, both of which have significant implications for overall health.

Recent years have witnessed a surge of studies highlighting the capacity of the gut microbiota and its metabolites to regulate skeletal muscle atrophy by engaging in skeletal muscle energy metabolism. This intricate process involves the modulation of pivotal factors, including glucose and lipid metabolism, as well as the expression of inflammatory markers, collectively termed the 'gut-muscle axis'[7]. The 'gut-muscle axis' hypothesis proposes that the gut microbiota and its interactions with the host's intestinal environment profoundly impact skeletal muscle metabolism and function[8]. For instance, animal models have demonstrated that systemic inflammation triggered by lipopolysaccharides (LPS) is often accompanied by intestinal barrier dysfunction and skeletal muscle atrophy[9,10]. Germ-free mice exhibit skeletal muscle atrophy, decreased expression of insulin-like growth factor 1, and downregulated transcription of genes associated with skeletal muscle growth and mitochondrial function[11]. Research has shown that the depletion of gut microbiota, or antibiotic-induced microbial dysbiosis, can lead to a reduction in skeletal muscle mass and cross-sectional area of muscle fibers. Additionally, these perturbations can alter the expression of skeletal muscle atrophy markers, such as FoxO, Atrogin-1, Murf-1, and MyoD, as well as genes related to skeletal muscle growth (ERK1/2, p90RSK, and RPS6) and mitochondrial function (PGC-1α and AMPK)[12–14]. In essence, a compelling correlation appears to exist between the gut microbiota and skeletal muscle mass, suggesting a profound interplay between these two systems.

Low-intensity pulsed ultrasound (LIPUS) has been established to stimulate tissue metabolism and expedite muscle healing processes[15]. Recently,

[1]Institute of Sports Biology, Shaanxi Normal University, Xi'an, China. [2]Shaanxi Key Laboratory of Ultrasonics, Shaanxi Normal University, Xi'an, China. [3]Center for Biomedical Engineering, School of Information Science and Technology, Fudan University, Shanghai, China. [4]Department of Rehabilitation Medicine, Huashan Hospital, Fudan University, Shanghai, China. ✉e-mail: sunlijun@snnu.edu.cn; tl531@snnu.edu.cn; tda@fudan.edu.cn

studies have shown that abdominal LIPUS can inhibit colonic inflammation induced by lipopolysaccharide (LPS) and alleviate LPS-induced inflammation by modulating TLR4/NF-κB signaling pathways and tight junction protein expression[16,17]. However, to date, there has been no report on whether LIPUS can prevent skeletal muscle atrophy by reversing intestinal microbial disorders in weightless conditions. If proven effective, LIPUS would not only address intestinal flora disorders but also safeguard against systemic skeletal muscle atrophy resulting from microgravity. Combining abdominal irradiation with direct irradiation of skeletal muscle may offer a novel strategy for the practical application of LIPUS in preventing skeletal muscle atrophy, especially in the context of long-term space flights.

Therefore, grounded in the concept of the gut-muscle axis, the objective of this study is to explore the impact of abdominal ultrasound LIPUS treatment on skeletal muscle atrophy, gut microbiota imbalance, and gut barrier defects in hindlimb unloaded mice. Furthermore, through fecal microbiota transplantation, we aim to demonstrate that abdominal LIPUS stimulation prevents skeletal muscle atrophy by ameliorating microbial dysbiosis.

Results

Abdominal LIPUS treatment improved muscle atrophy in hindlimb unloaded mice

Figure 1A depicts hindlimb unloaded mice undergoing 28 days of abdominal ultrasound treatment, specifically LIPUS. As illustrated in Fig. 1B–E, when compared to the normal control (NC) group, the hindlimb unloaded (HU) group exhibited a marked decline in body weight, muscle weight, and grip strength ($p < 0.01$ for all). Conversely, the HU + LIPUS group showed a significant increase in body weight, muscle weight and grip strength ($p < 0.01$, $p < 0.01$, $p < 0.05$ and $p < 0.01$). Histological examination revealed notable changes in muscle fiber morphology (Fig. 1F). Specifically, the HU group displayed a reduction or dissolution of muscle fibers within the skeletal muscle, accompanied by disorganized muscle fiber arrangement and inflammatory cell infiltration into the stroma. This was further confirmed by a significant decrease in the mean cross-sectional area of muscle fibers in the HU group compared to the NC group ($p < 0.01$), particularly within the range of 300–600 μm². In contrast, the HU + LIPUS group exhibited a tighter and more regular muscle bundle structure, with a clear and intact fascia, and a significant increase in the average fiber cross-sectional area compared to the HU group ($p < 0.01$), particularly within the range of 600–900 μm². (Fig. 1G, H). Functional assessments of the gastrocnemius muscle further supported these findings. As shown in Fig. 1I, J, in vivo and in situ gastrocnemius muscle contraction was significantly reduced in the HU group compared to the NC group (both $p < 0.01$). However, the HU + LIPUS group demonstrated a significant increase in both in vivo and in situ gastrocnemius muscle contraction compared to the HU group (both $p < 0.01$). Biochemical markers of muscle damage, including lactate dehydrogenase (LDH) and creatine kinase (CK) activities were also evaluated (Fig. 1K, L). The HU group showed a significant increase in both LDH and CK activities compared to the NC group (both $p < 0.01$). Importantly, the HU + LIPUS group exhibited a significant decrease in these markers compared to the HU group (both $p < 0.01$), suggesting a protective effect of abdominal LIPUS on muscle damage. Finally, behavioral assessments of motor function were conducted (Fig. 1M–O). Compared to the NC group, the HU group showed a significant decrease in latency to fall off, speed, and total distance traveled ($p < 0.01$ for all). However, the HU + LIPUS group demonstrated a significant improvement in these parameters compared to the HU group ($p < 0.01$ for all), indicating an enhancement in exercise ability following abdominal LIPUS treatment.

The effect of abdominal LIPUS on the MSTN/AKT/mTOR signaling pathway in hindlimb unloaded mice

As illustrated in Fig. 2A, B, the protein expression levels of MSTN and ActRIIB were significantly upregulated in the HU group compared to the NC group (both $p < 0.01$). Conversely, in the HU + LIPUS group, the protein expression levels of MSTN and ActRIIB were notably downregulated compared to the HU group ($p < 0.01$ and $p < 0.05$, respectively). Figure 2C, D demonstrates that the protein expression levels of AKT and mTOR were significantly downregulated in the HU group compared to the NC group (both $p < 0.01$). However, in the HU + LIPUS group, the protein expression levels of AKT and mTOR were significantly upregulated compared to the HU group (both $p < 0.05$). These findings indicate that abdominal LIPUS may effectively suppress the protein expression of the muscle growth inhibitor MSTN, activate the expression of skeletal muscle growth factors AKT and mTOR, and thereby mitigate muscle atrophy. The original images are presented in Supplementary Table 1, and the corresponding antibody information is detailed in Supplementary Table 3.

Abdominal LIPUS treatment improved intestinal barrier and function in hindlimb unloaded mice

Histopathological examination of H&E-stained sections was conducted to assess the degree of injury in the small intestine and colon (Fig. 3A, H). Compared to the NC group, mice in the HU group exhibited pronounced mucosal abnormalities, including disrupted intestinal crypt structures, lack of clarity in the crypts, significant inflammatory cell infiltration, and marked fibrosis changes in the intestine. In contrast, mice in the HU + LIPUS group showed well-organized intestinal villi structures, smooth surfaces, and clear structural integrity. As illustrated in Fig. 3B–E, compared to the NC group, the HU group demonstrated a significant decrease in villi length, crypt depth, and the V/C ratio ($p < 0.01$ for all), accompanied by a significant increase in the villi rupture ratio ($p < 0.01$). In comparison to the HU group, the HU + LIPUS group exhibited a significant increase in villi length, crypt depth, and the V/C ratio ($p < 0.01$ for all), along with a significant decrease in the villi rupture ratio ($p < 0.01$).

The length and appearance changes of the colon can serve as indicators of the inflammatory response in colitis (Fig. 3F, G). Compared to the NC group, the colon length of the HU group was significantly reduced ($p < 0.01$). In contrast, the colon length of the HU + LIPUS group was significantly increased compared to the HU group ($p < 0.01$). H&E staining of the colon revealed fewer colonic folds, a looser lamina propria, and notable inflammatory cell infiltration in the HU group compared to the NC group. In comparison to the HU group, the HU + LIPUS group showed intact colon tissue structure, smooth intestinal mucosa, clear layer structure, neatly arranged intestinal villi and crypt structures, and no apparent inflammatory cell infiltration (Fig. 3H). As shown in Fig. 3I, compared to the NC group, the intestinal thickness of the HU group was significantly decreased ($p < 0.01$). Conversely, the intestinal thickness of the HU + LIPUS group was significantly increased compared to the HU group ($p < 0.01$).

As depicted in Fig. 3J, K, the fecal water content and maximum tensile load of the intestine in the HU group were significantly decreased compared to the NC group ($p < 0.01$ for both). In contrast, the HU + LIPUS group exhibited a significant increase in both fecal water content and maximum tensile load of the intestine compared to the HU group ($p < 0.01$ for both). Furthermore, there was no significant alteration in water intake, and the discrepancy in fecal water content was not attributable to the amount of water ingested (Supplementary Fig. 1).

To assess the integrity of the intestinal barrier, the protein expression levels of ZO-1 and Occludin were quantified (Fig. 3L, M). The results revealed that, compared to the NC group, the protein expression levels of both Occludin and ZO-1 were significantly downregulated in the HU group ($p < 0.01$ and $p < 0.01$, respectively). However, in comparison to the HU group, the HU + LIPUS group showed a significant upregulation in the protein expression levels of Occludin and ZO-1 ($p < 0.01$ and $p < 0.05$, respectively). The original WB images are presented in Supplementary Table 1, and the corresponding antibody information is detailed in Supplementary Table 3.

As illustrated in Fig. 3N, the LPS activity in the HU group was significantly elevated compared to the NC group ($p < 0.01$). Conversely, the LPS activity in the HU + LIPUS group was significantly reduced compared to the HU group ($p < 0.01$). In conclusion, abdominal LIPUS can effectively

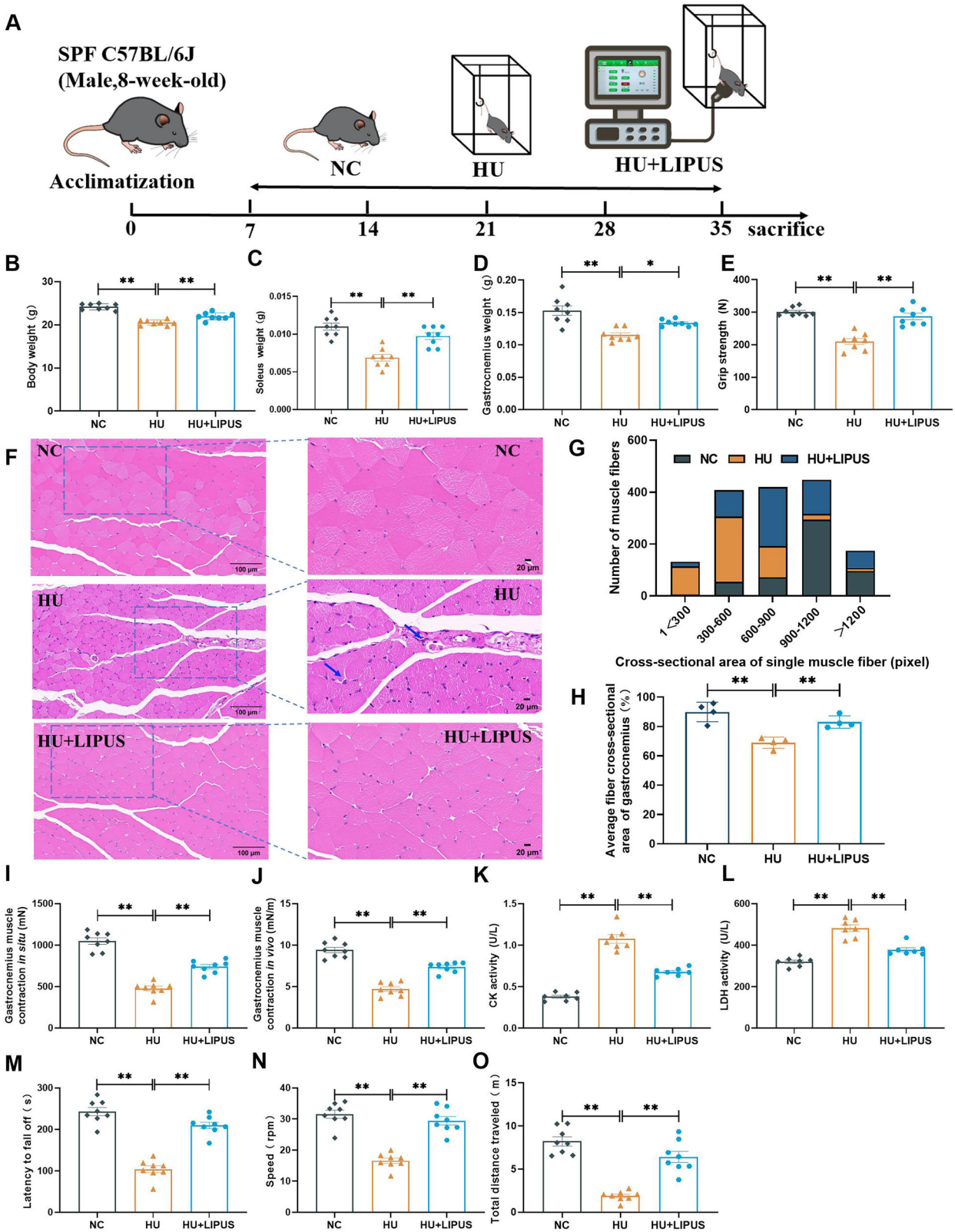

Fig. 1 | The effect of abdominal LIPUS treatment on muscle atrophy in hindlimb unloaded mice. **A** Diagram of the ultrasound intervention protocol. **B** Body weight. **C** Soleus muscle weight. **D** Gastrocnemius muscle weight. **E** Grip strength. **F** Hematoxylin-eosin staining. **G** Distribution of muscle fiber area ($n = 4$). **H** Average fiber cross-sectional area of gastrocnemius. **I** Gastrocnemius muscle contraction in situ. **J** Gastrocnemius muscle contraction in vivo. **K** CK activity. **L** LDH activity. **M** Latency to fall off. **N** Speed. **O** Total distance traveled. The data were expressed as mean ± SD, $^{*}p < 0.05$ and $^{**}p < 0.01$.

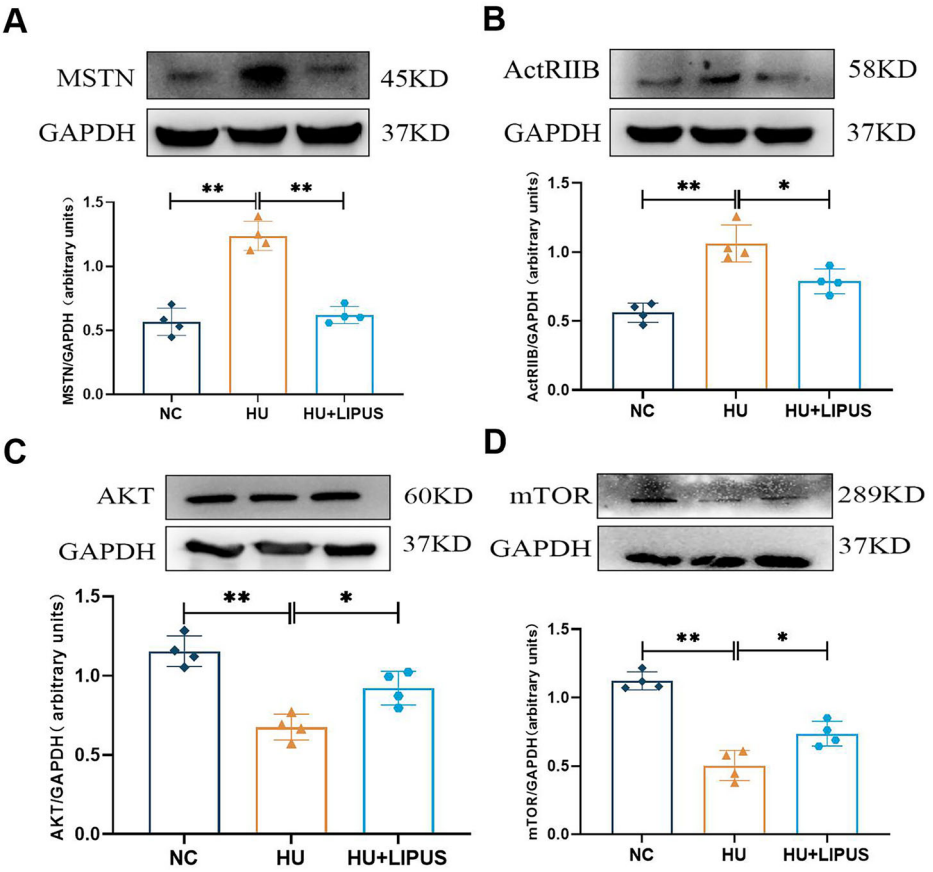

Fig. 2 | The effect of abdominal ultrasound on the MSTN/AKT/mTOR signaling pathway in hindlimb unloaded mice. A The protein level of MSTN in gastrocnemius muscle. **B** The protein level of ActRIIB in gastrocnemius muscle. **C** The protein level of AKT in gastrocnemius muscle. **D** The protein level of mTOR in gastrocnemius muscle. The data were expressed as mean ± SD, $^{*}p < 0.05$ and $^{**}p < 0.01$.

prevent damage to the intestinal barrier, ensure intestinal integrity, and mitigate intestinal leakage.

Abdominal LIPUS treatment modulates gut microbiota distribution in hindlimb unloaded mice

The Venn diagram in Fig. 4A demonstrates the distribution of gene abundances among the experimental groups, revealing a total of 4918 identified genes. Specifically, 430 genes were exclusive to the NC group, 679 were unique to the HU group, and 286 were specific to the HU + LIPUS group. Notably, there were 1082 genes common to both the NC and HU groups, and 960 genes shared between the HU and HU + LIPUS groups. Additionally, 741 genes were present across all three groups.

Alpha diversity analysis, which quantifies species diversity within a given biological environment, is depicted in Fig. 4B, C. When compared to the NC group, the HU group exhibited a 33% increase in the Chao 1 index, indicative of higher species richness, and a statistically significant elevation in the Shannon index ($p < 0.05$), suggesting greater species diversity. Conversely, in comparison to the HU group, the HU + LIPUS group demonstrated a 29% decrease in the Chao 1 index and a notable reduction in the Shannon index ($p < 0.05$), pointing towards a decrease in both species' richness and diversity.

Principal component analysis (PCA), shown in Fig. 4D, revealed marked differences in microbial community composition between the NC and HU groups. Interestingly, the HU + LIPUS group exhibited a microbial community profile that was remarkably similar to that of the NC group, indicating a potential normalization effect of the Abdominal LIPUS treatment on the gut microbiota of hindlimb unloaded mice.

To elucidate the distinct alterations in gut microbiota, a comparative analysis was undertaken, focusing on the relative abundance of key taxonomic groups identified through sequencing across three distinct groups. At the phylum level, when compared to the NC group, the HU group exhibited a notable 15% decline in the relative abundance of *Bacteroidetes*, a substantial 28% increase in *Firmicutes*, and a striking 57% reduction in *Epsilonbacteraeota*. Consequently, the *Firmicutes*-to-*Bacteroidetes* ratio rose in the HU group. Conversely, in comparison to the HU group, the HU + LIPUS group demonstrated a significant 29% increase in *Bacteroidetes*, a 34% decrease in *Firmicutes*, and a 38% elevation in *Epsilonbacteraeota*, resulting in a decrease in the *Firmicutes*-to-*Bacteroidetes* ratio within the HU + LIPUS group (Fig. 4E).

At the genus level, the HU group showed a marked 60% decrease in the relative abundance of *Bacteroides* compared to the NC group, accompanied by a 57% drop in *Parabacteroides* and a surge 55% in *Alloprevotella*. In contrast, the HU + LIPUS group exhibited a notable increase in the relative abundance of *Bacteroides* compared to the HU group, along with a 56% elevation in *Parabacteroides* and a 45% decrease in *Alloprevotella* (Fig. 4F). These findings underscored the profound influence of abdominal LIPUS treatment on the gut microbiota composition in mice.

Prediction of potential metabolic functions of gut microbiota in mice

As depicted in Fig. 5A–C, the PICRUSt2 software, leveraging the KEGG database, was employed to predict the functional capabilities of the gut microbiota. The KEGG pathway classification system is hierarchical, comprising three levels. At Level 1, six broad categories are identified at the apex: cellular processes, environmental information processing, genetic information processing, human diseases, metabolism, and organismal systems. At Level 2, a total of ten enriched subcategories are highlighted. When compared to the NC group, the HU group exhibited decreases in membrane transport, carbohydrate metabolism, amino acid metabolism, replication and repair, and energy metabolism, albeit none of these changes reached statistical significance. Conversely, in comparison to the HU group, the HU + LIPUS group displayed increases in these same metabolic categories, yet again without achieving statistical significance.

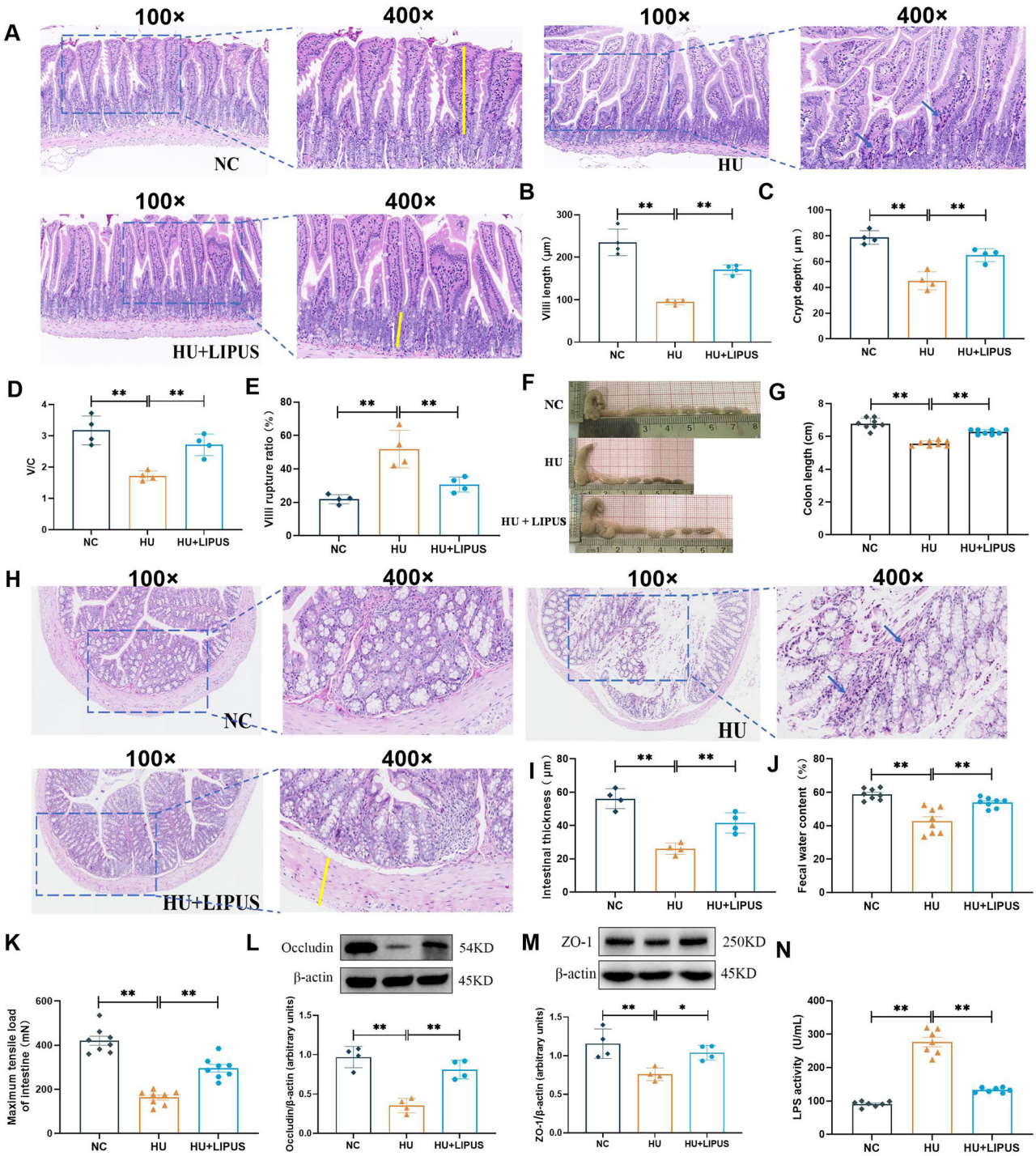

Fig. 3 | The effect of abdominal LIPUS treatment on intestinal barrier and function in hindlimb unloaded mice. **A** HE staining of small intestinal tissue. **B** Villi length. **C** Crypt depth. **D** Villi length/Crypt depth. **E** Villi rupture ratio. **F** Representative images of the colon of mice. **G** Colon length. **I** Intestinal thickness. **H** HE staining of colonic tissues. **J** Fecal water content. **K** Maximum tensile load of intestine. **L** The protein level of Occludin in colon. **M** The protein level of ZO-1 in colon. **N** LPS activity. The data were expressed as mean ± SD, $^{*}p < 0.05$ and $^{**}p < 0.01$.

Upon further scrutiny at KEGG Level 3, numerous additional pathways emerged. Specifically, at this level, ten enriched subcategories were prominent. When compared to the NC group, the HU group showed increases in transporters, general function prediction only, ABC transporters, DNA repair and recombination proteins, and ribosome, although these increases were not statistically significant. In contrast, when compared to the HU group, the HU + LIPUS group exhibited decreases in membrane transport, carbohydrate metabolism, amino acid metabolism, replication and repair, and energy metabolism, once more without reaching statistical significance.

Abdominal LIPUS treatment enhances SCFA concentrations in hindlimb unloaded mice

To delve deeper into the regulatory impact of abdominal LIPUS on microbial metabolites, we measured the concentration of short-chain fatty acids (SCFAs) in colon contents. As illustrated in Fig. 6A–G, compared to

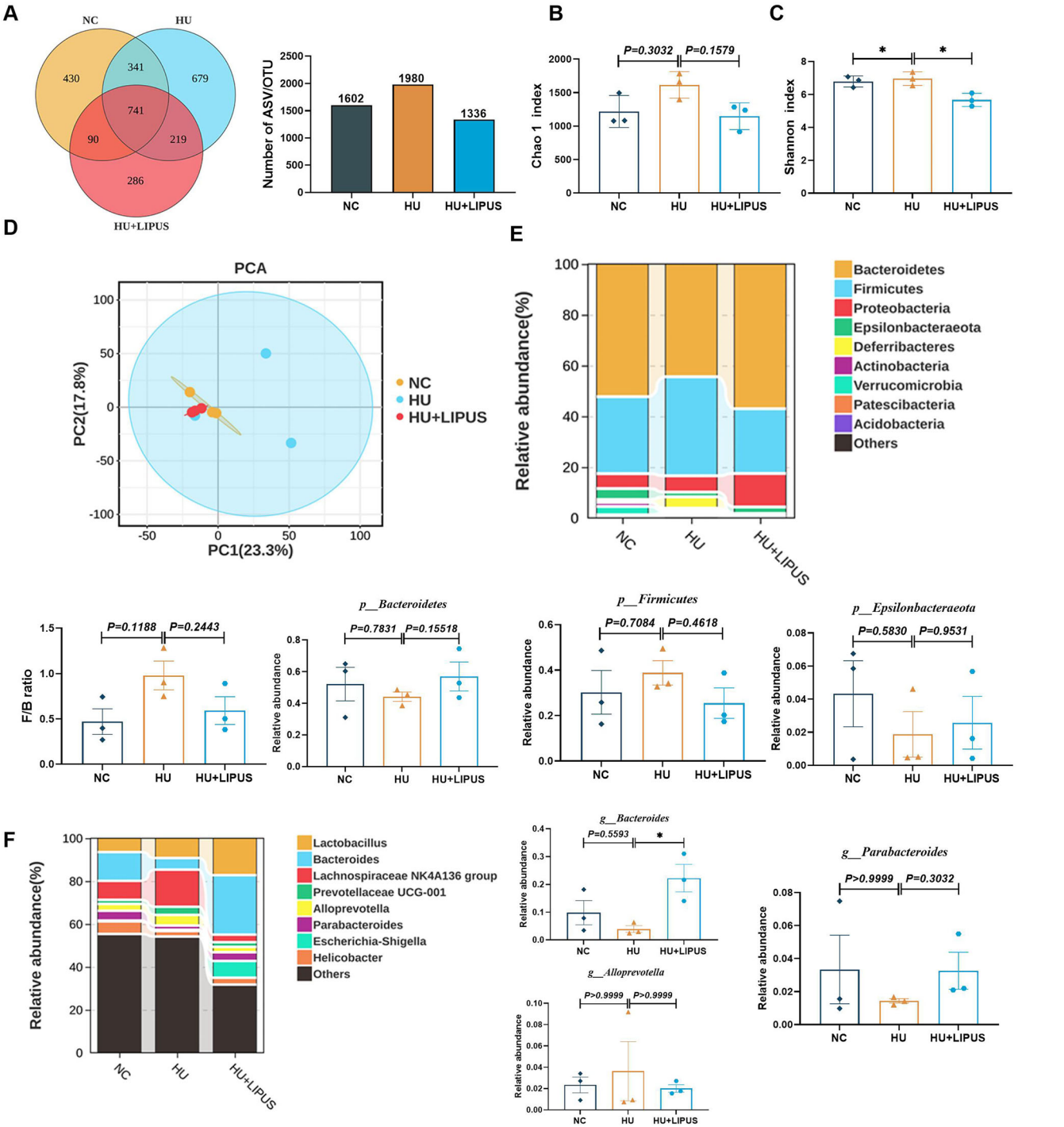

Fig. 4 | The effect of abdominal LIPUS treatment on gut microbiota in hindlimb unloaded mice. A Differences in the distribution of OTUs between groups using the Venn diagram. **B** Chao 1 index. **C** Shannon index. **D** Principal component analysis (PCA). **E** Gut bacterial composition at the phylum level. **F** Gut bacterial composition at the genus level. The relative abundance of top 10 genus. The data were expressed as mean ± SD, $^{*}p < 0.05$ and $^{**}p < 0.01$.

the NC group, the HU group exhibited a significant reduction in acetic acid ($p < 0.05$), propionic acid (37% decrease), isobutyric acid (43% decrease), butyric acid ($p < 0.01$), isovaleric acid (36% decrease), and valeric acid (20% decrease). In contrast, the HU + LIPUS group showed a marked increase in propionic acid and butyric acid levels compared to the HU group (both $p < 0.01$). Similarly, the content of acetic acid increased by 40%, isobutyric acid by 45%, isovaleric acid by 3%, and valeric acid by 34% in the HU + LIPUS group. These findings suggest that LIPUS promotes the production of SCFAs. Figure 6H presents the correlation analysis between gut microbiota, the metabolic products SCFAs, skeletal muscle function, and MSTN. Association analysis revealed that acetic acid, isobutyric acid, and butyric acid were significantly correlated with skeletal muscle function indicators and MSTN.

Fecal microbiota transplantation from abdominal LIPUS-treated mice alleviates muscle atrophy in hindlimb unloaded mice

Hindlimb unloaded mice underwent fecal microbiota therapy, as depicted in Fig. 7A. As illustrated in Fig. 7B, E, when compared to the HU FMT NaCl group, the HU FMT LIPUS group exhibited significant increases in body weight and gastrocnemius muscle weight ($p < 0.05$ and $p < 0.01$). Similarly,

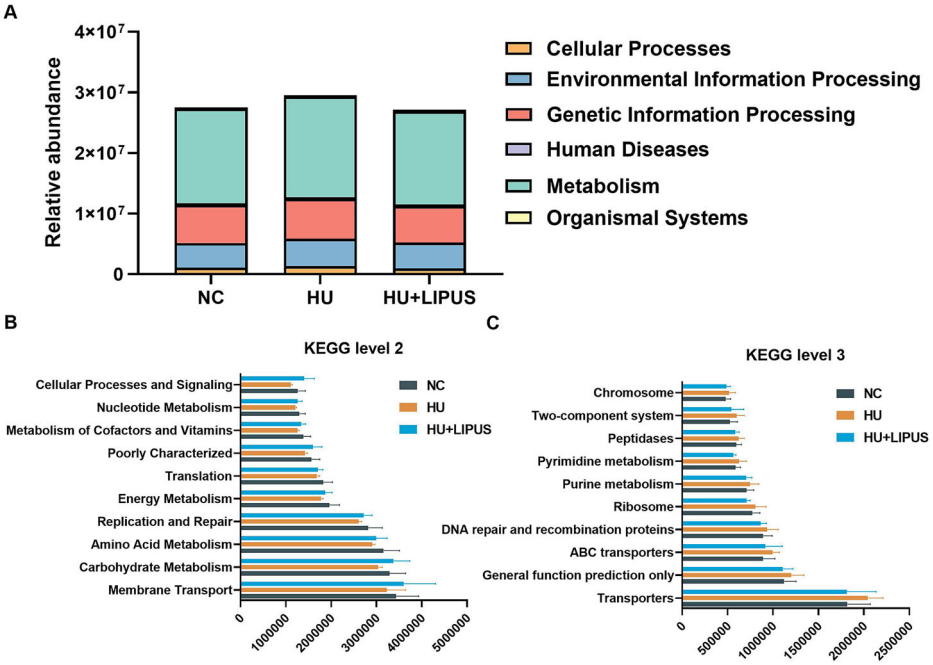

Fig. 5 | Prediction of gut microbiota function by KEGG. A Relative abundance of biological entities and characteristics. **B** KEGG function level 2. **C** KEGG function level 3. The data were expressed as mean ± SD ($n = 3$).

both the HU FMT WT group and the HU FMT LIPUS group demonstrated significant elevations in soleus muscle weight and grip strength compared to the HU FMT NaCl group (both $p < 0.01$). Notably, the HU FMT LIPUS group showed further significant increases in soleus muscle weight and grip strength when compared to the HU FMT WT group ($p < 0.05$ and $p < 0.01$).

Figure 7F–H reveal that, in contrast to the HU FMT NaCl group, the muscle bundles in both the HU FMT WT and HU FMT LIPUS groups displayed a tighter and more organized structure, with a clear and intact fascia. Additionally, average fiber cross-sectional area of gastrocnemius was significantly larger in these groups ($p < 0.05$ and $p < 0.01$). When compared to the HU FMT WT group, the average fiber cross-sectional area in the HU FMT LIPUS group exhibited an 8% increase. In the HU FMT NaCl group, the specific muscle fiber cross-sectional area was predominantly within the range of 300–600 μm^2, whereas in the HU FMT WT and HU FMT LIPUS groups, the predominant range was 600–900 μm^2. Notably, compared to the HU FMT WT group, the HU FMT LIPUS group exhibited a higher number of fibers with a cross-sectional area exceeding 1200 μm^2.

As shown in Fig. 7I, J, both in situ and in vivo gastrocnemius muscle contraction increased in the HU FMT WT and HU FMT LIPUS groups compared to the HU FMT NaCl group ($p = 0.01$, $p < 0.01$; $p < 0.05$ and $p < 0.01$). Furthermore, the HU FMT LIPUS group exhibited significantly higher gastrocnemius muscle contraction than the HU FMT WT group, both in situ and in vivo ($p < 0.05$ for all).

Figure 7K, L indicates that, compared to the HU FMT NaCl group, creatine kinase (CK) and lactate dehydrogenase (LDH) activities were significantly decreased in both the HU FMT WT and HU FMT LIPUS groups ($p < 0.01$, $p < 0.01$; $p < 0.05$, $p < 0.01$). When compared to the HU FMT WT group, the CK activity in the HU FMT LIPUS group was further decreased ($p < 0.05$).

Finally, Fig. 7N, O demonstrates that, in comparison to the HU FMT NaCl group, both the HU FMT WT and HU FMT LIPUS groups showed significant improvements in latency to fall off, speed, and total distance traveled ($p < 0.01$, $p < 0.01$; $p < 0.05$, $p < 0.01$; $p < 0.01$, $p < 0.01$). Furthermore, the HU FMT LIPUS group exhibited significantly better performance in these parameters when compared to the HU FMT WT group ($p < 0.01$ for all).

The above results indicated that fecal microbiota transplantation from LIPUS-treated mice can effectively alleviate muscle atrophy in hindlimb unloaded mice.

The effect of fecal microbiota transplantation from abdominal LIPUS treated mice on the MSTN/AKT/mTOR signaling pathway in hindlimb unloaded mice

As illustrated in Fig. 8A, B, the HU FMT NaCl group exhibited significantly higher protein expression levels of MSTN and ActRIIB compared to both the HU FMT WT group and the HU FMT LIPUS group ($p < 0.05$, $p < 0.01$; $p < 0.01$, $p < 0.01$. Furthermore, within the context of comparison between the HU FMT WT and HU FMT LIPUS groups, the protein expression levels of MSTN and ActRIIB were notably downregulated in the HU FMT LIPUS group ($p < 0.05$, $p < 0.05$, respectively). In Fig. 8C, D, compared with the HU FMT NaCl group, the protein expression levels of AKT and mTOR in the HU FMT WT group and HU FMT LIPUS group were upregulated ($p = 0.4687$, $p < 0.01$; $p = 0.1493$, $p < 0.05$). When comparing the HU FMT WT and HU FMT LIPUS groups, the protein expression levels of AKT and mTOR showed a trend towards upregulation in the HU FMT LIPUS group, albeit without reaching statistical significance (($p = 0.2123$, $p = 0.2065$, respectively). These findings indicated that fecal microbiota transplantation from mice treated with abdominal LIPUS may effectively suppress the expression of MSTN, a muscle growth inhibitor, while enhancing the expression of AKT and mTOR, skeletal muscle growth factors, thereby potentially mitigating muscle atrophy. The original images are presented in Supplementary Table 2, and the corresponding antibody information is detailed in Supplementary Table 3.

Fecal microbiota transplantation from abdominal LIPUS treated mice improved intestinal barrier and function in hindlimb unloaded mice

The HU FMT NaCl group exhibited notable mucosal defects in the small intestine, characterized by unclear or absent crypt structures, substantial infiltration of inflammatory cells, and pronounced intestinal fibrosis. In contrast, both the HU FMT WT group and the HU FMT LIPUS group displayed well-organized villous structures in the small intestine, with smooth surfaces and clear, defined structures (Fig. 9A).

As illustrated in Fig. 9B–E, compared to the HU FMT NaCl group, the HU FMT WT and HU FMT LIPUS groups exhibited significant increases in villi length, crypt depth, and the villi length-to-crypt depth ratio ($p < 0.01$, $p < 0.01$; $p < 0.01$, $p < 0.01$; $p < 0.05$, $p < 0.01$). Additionally, there was a notable decrease in the villi rupture ratio in both groups ($p < 0.01$ for both). When comparing the HU FMT WT and HU FMT LIPUS groups, the latter

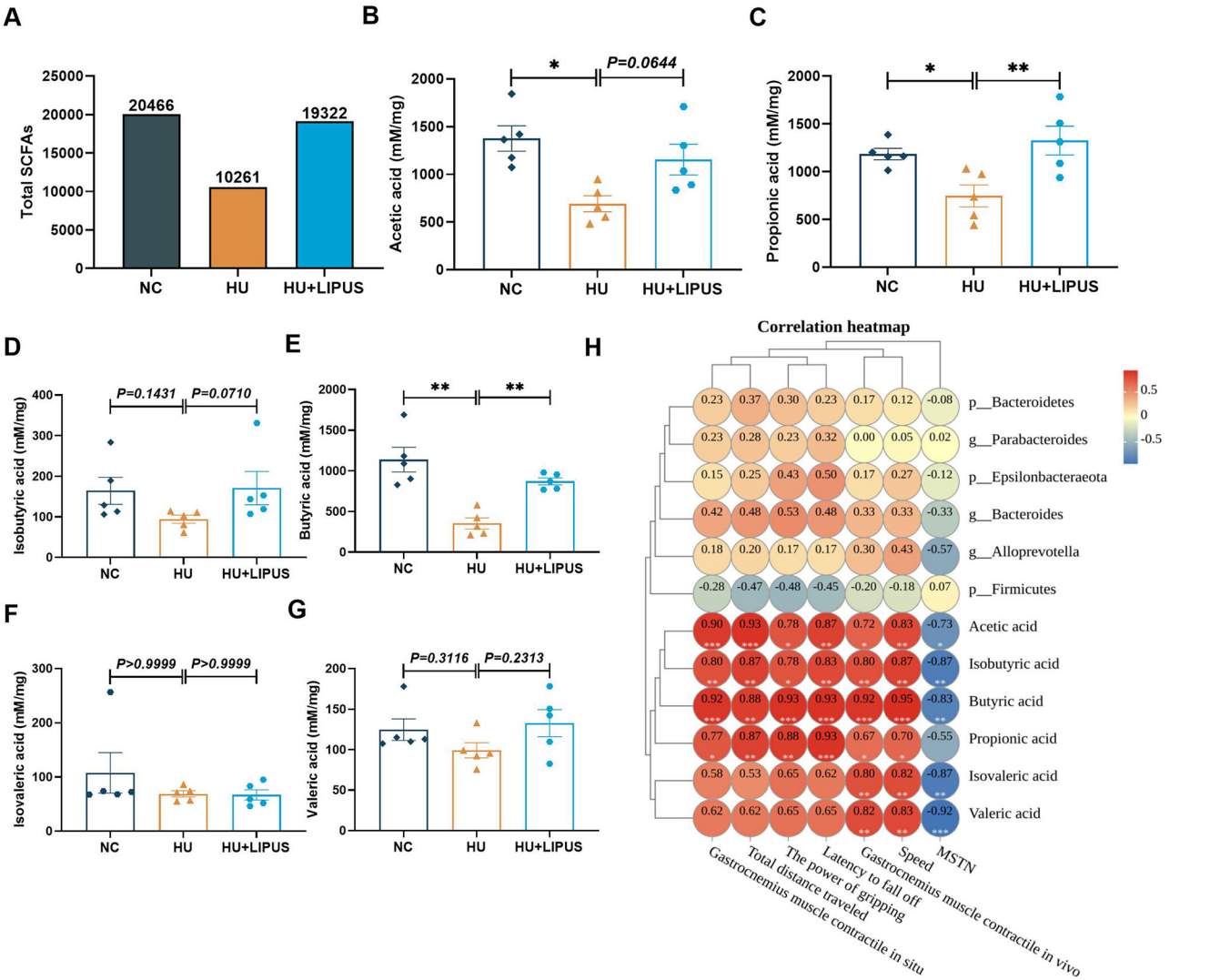

Fig. 6 | The effect of abdominal LIPUS treatment on SCFAs in hindlimb unloaded mice. **A** Total SCFAs. **B** Acetic acid. **C** Propionic acid. **D** Isobutyric acid. **E** Butyric acid. **F** Isovaleric acid. **G** Valeric acid. **H** Correlation analysis between the structural composition of gut microbiota and skeletal muscle functional indicators ($n = 3$). The data were expressed as mean ± SD, $^{*}p < 0.05$ and $^{**}p < 0.01$.

showed further significant increases in villi length, crypt depth, and the villi length-to-crypt depth ratio ($p < 0.01$ for all), along with a decreased villi rupture ratio ($p < 0.01$).

Changes in colon length and appearance can serve as indicators of colitis-related inflammation (Fig. 9F, G). Compared to the HU FMT NaCl group, both the HU FMT WT and HU FMT LIPUS groups exhibited significant increases in colon length ($p < 0.05$ and $p < 0.01$, respectively). Furthermore, the HU FMT LIPUS group showed an additional increase in colon length compared to the HU FMT WT group. HE staining of the colon revealed that the HU FMT NaCl group had fewer colonic folds, a looser lamina propria, and significant inflammatory cell infiltration. In contrast, both the HU FMT WT and HU FMT LIPUS groups displayed intact colonic tissue structures, smooth intestinal mucosa, clear layer structures, neatly arranged intestinal villi and crypt structures, and minimal inflammatory cell infiltration (Fig. 9H).

As shown in Fig. 9I, compared to the HU FMT NaCl group, both the HU FMT WT and HU FMT LIPUS groups exhibited significant increases in intestinal thickness (both $p < 0.01$). Moreover, the HU FMT LIPUS group showed a further significant increase in intestinal thickness compared to the HU FMT WT group ($p < 0.01$). These findings suggest that FMT from mice treated with abdominal LIPUS can effectively enhance intestinal barrier function, improve intestinal morphology, and reduce inflammation, thereby contributing to overall intestinal health in HU mice.

As depicted in Fig. 9J, K, the fecal water content and maximum tensile load of the intestine in both the HU FMT WT group and HU FMT LIPUS group exhibited significant increases when compared to the HU FMT NaCl group ($p < 0.01$ for all comparisons). Furthermore, when comparing the HU FMT LIPUS group to the HU FMT WT group, notable elevations were also observed in both fecal water content and maximum tensile load of the intestine ($p < 0.05$ and $p < 0.01$, respectively). Furthermore, the results obtained demonstrate that there was no significant alteration in water intake, and the discrepancy in fecal water content was not attributable to the amount of water ingested (Supplementary Fig. 1).

To assess the integrity of the intestinal barrier, the protein expression levels of Occludin and ZO-1 were quantified (Fig. 9L, M). Both the HU FMT WT and HU FMT LIPUS groups demonstrated significant upregulation in the protein expression levels of Occludin and ZO-1 compared to the HU FMT NaCl group ($p < 0.05$, $p < 0.01$; $p < 0.05$ and $p < 0.01$). Additionally, the HU FMT LIPUS group showed an upregulation in the protein expression levels of these tight junction proteins compared to the HU FMT WT group, with statistical significance for Occludin and ZO-1 ($p < 0.05$ and $p < 0.01$, respectively). The original WB images are presented in Supplementary

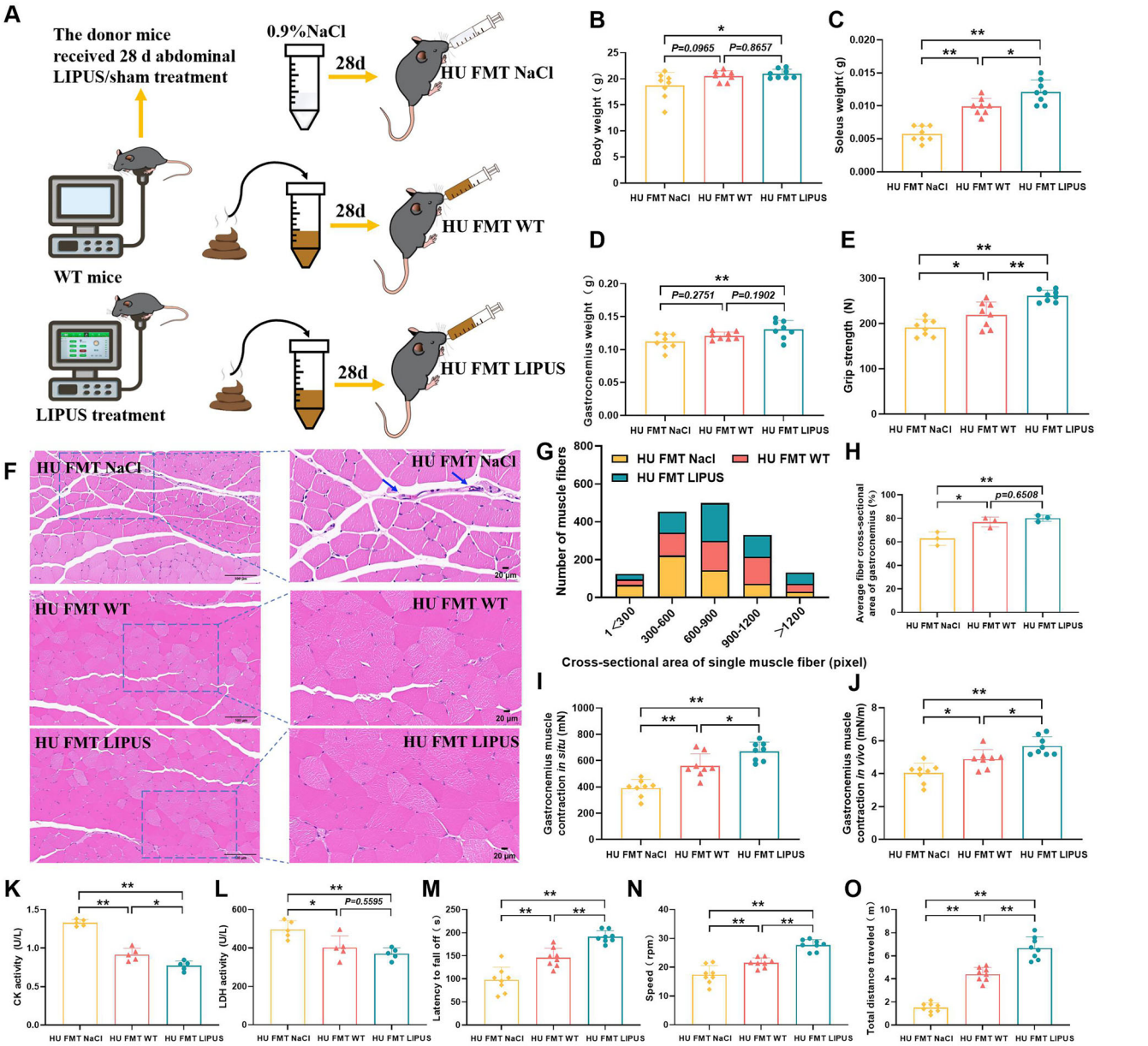

Fig. 7 | The effect of fecal microbiota transplantation from abdominal LIPUS treated mice on muscle atrophy in hindlimb unloaded mice. **A** Diagram of the ultrasound intervention protocol. **B** Body weight. **C** Soleus muscle weight. **D** Gastrocnemius muscle weight. **E** Grip strength. **F** Hematoxylin and eosin staining. **G** Distribution of muscle fiber area ($n = 4$). **H** Average fiber cross-sectional area of gastrocnemius. **I** Gastrocnemius muscle contraction in situ. **J** Gastrocnemius muscle contraction in vivo. **K** CK activity. **L** LDH activity. **M** Latency to fall off. **N** Speed. **O** Total distance traveled. The data were expressed as mean ± SD, $^{*}p < 0.05$ and $^{**}p < 0.01$.

Table 2, and the corresponding antibody information is detailed in Supplementary Table 3. As illustrated in Fig. 9N, the LPS activity in both the HU FMT WT and HU FMT LIPUS groups was markedly reduced when compared to the HU FMT NaCl group ($p < 0.01$ for both). Notably, the HU FMT LIPUS group exhibited a further significant decrease in LPS activity compared to the HU FMT WT group ($p < 0.01$). In summary, fecal microbiota transplantation sourced from mice undergoing abdominal LIPUS treatment can effectively prevent intestinal barrier damage, safeguard intestinal integrity, and mitigate intestinal leakage.

Fecal microbiota transplantation from abdominal LIPUS treated mice increased production of SCFAs in hindlimb unloaded mice

The influence of fecal microbiota transplantation (FMT) on the concentrations of short-chain fatty acids (SCFAs) in hindlimb unloaded (HU) mice is illustrated in Fig. 10A–G. When compared to the HU FMT NaCl group, the HU FMT WT group exhibited a 45% increase in acetic acid content, a 48% rise in propionic acid content, a 37% augmentation in isobutyric acid content, a 47% boost in butyric acid content, a statistically significant elevation in isovaleric acid content ($p < 0.05$), and a 44% increase in valeric acid content. The HU FMT LIPUS group, on the other hand, demonstrated a 51% increase in acetic acid, a 32% increase in propionic acid, statistically significant increments in isobutyric acid ($p < 0.05$) and butyric acid ($p < 0.01$), a significant elevation in isovaleric acid ($p < 0.05$), and a significant rise in valeric acid ($p < 0.05$). Furthermore, when compared to the HU FMT WT group, the HU FMT LIPUS group showed a 13% increase in acetic acid content, a 43% increase in propionic acid content, a 12% augmentation in isobutyric acid content, a statistically significant elevation in butyric acid ($p < 0.05$), a 3% increase in isovaleric acid content, and a 38% increase in valeric acid content. These findings suggest that FMT sourced from mice undergoing abdominal LIPUS treatment promotes the

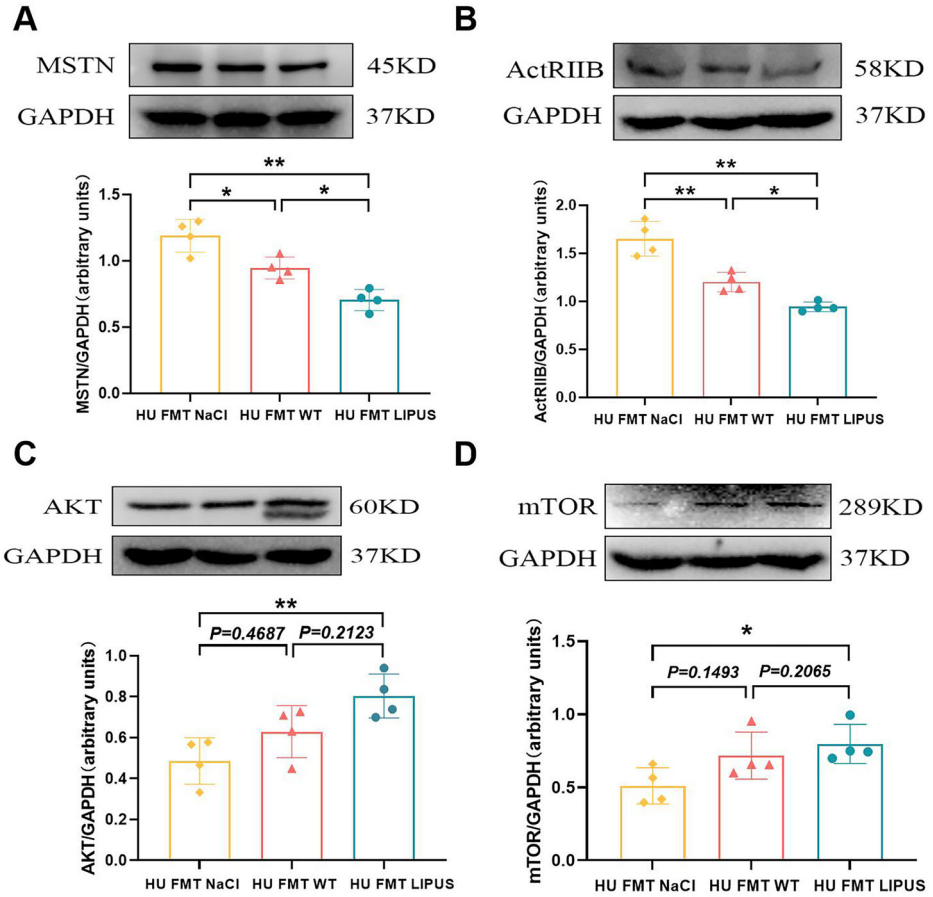

Fig. 8 | The effect of fecal microbiota transplantation from abdominal LIPUS treated mice on the MSTN/AKT/mTOR signaling pathway in hindlimb unloaded mice. A The protein level of MSTN in gastrocnemius muscle. **B** The protein level of ActRIIB in gastrocnemius muscle. **C** The protein level of AKT in gastrocnemius muscle. **D** The protein level of mTOR in gastrocnemius muscle. The data were expressed as mean ± SD, $^{*}p < 0.05$ and $^{**}p < 0.01$.

production of SCFAs. The correlation analysis between SCFAs, skeletal muscle function, and myostatin (MSTN) is presented in Fig. 10H. The analysis revealed significant correlations between SCFAs and indicators of skeletal muscle function as well as MSTN.

Discussions

Long term exposure to microgravity environment or lack of mechanical stimulation can lead to skeletal muscle atrophy and intestinal microbiota imbalance[18,19]. Consequently, identifying methods to prevent muscle atrophy in such environments is of paramount importance[20]. In recent years, great breakthroughs have been made in the research on the gut-muscle axis[21]. Therefore, we conducted an investigation to determine whether abdominal Low-Intensity Pulsed Ultrasound (LIPUS) could mitigate the gut microbiota dysbiosis and skeletal muscle atrophy caused by hindlimb unloading. Our results indicated that abdominal LIPUS effectively alleviated the intestinal microbiota imbalance and skeletal muscle atrophy resulting from hindlimb unloading. Additionally, similar benefits were observed through intestinal microbiota transplantation.

Microgravity can exert profound effects on microbial growth and metabolism[22]. An elevated *Firmicutes* to *Bacteroidetes* (F/B) ratio has emerged as a potential biomarker of ecological imbalance. A study conducted on mice that underwent a 37-day spaceflight aboard the International Space Station (ISS) revealed an increase in this ratio, accompanied by an augmentation in both the Shannon index and alpha diversity[23]. In this study, after 28 days of hindlimb unloading, the F/B ratio of the mice increased, indicating a disruption in gut microbiota balance. Additionally, there was an increase in the Chao 1 index and Shannon index, suggesting an enhancement in microbial alpha diversity. Spaceflight has the capacity to modify the abundance of gut microbiota, thereby compromising its stability. For instance, the NASA Twins Study, which involved a 340-day space mission, demonstrated significant differences in the fecal microbiota of the participants[18]. Moreover, spaceflight led to substantial alterations in the abundance of microbes at the order, family, genus, and species levels[24]. Similarly, both spaceflight and ground-based microgravity simulations have shown an increase in *Firmicutes* and a decrease in *Bacteroidetes*[25,26]. The absence of gravity has also been shown to decrease the abundance of beneficial gut bacteria, such as *Bifidobacteria*, while concurrently increasing the abundance of opportunistic pathogens, like *Escherichia coli*[27]. Our research findings indicate that the hindlimb unloaded (HU) group exhibited an increased abundance of *Firmicutes* and a decreased abundance of *Bacteroidetes*. Furthermore, there was a reduction in the relative abundance of *Parabacteroides* and an increase in *Alloprevotella* in the HU group. *Parabacteroides*, a core member of the human gut microbiota with an average abundance of 1.27% across 12 diverse human populations, are closely associated with host health, including metabolic syndrome, inflammatory bowel disease, and obesity, and have demonstrated efficacy in alleviating inflammatory arthritis[28]. *Alloprevotella* is an obligate anaerobic, Gram-negative bacterium. Studies on bacterial carcinogenesis in the oral cavity have reported a significant increase in the abundance of the *Alloprevotella* genus[29,30]. Therefore, microgravity may alter the composition of gut microbiota, leading to dysbiosis. However, following abdominal LIPUS intervention, the microbiota composition in colonic contents was restored. This was evidenced by a decrease in the relative abundance of *Firmicutes*, an increase in the relative abundance of *Bacteroidetes*, a decline in the F/B ratio, a reduction in species richness and diversity, an increase in the relative abundance of *Parabacteroides*, and a decrease in the abundance of *Alloprevotella*. These results suggest that abdominal LIPUS treatment could reverse the intestinal microbiota disorder caused by hindlimb unloading.

The gut microbiota plays a crucial role in maintaining optimal intestinal morphology and barrier function[31]. Microgravity conditions, however, have the potential to disrupt these morphological features and barrier integrity, leading to the infiltration of inflammation within the gut

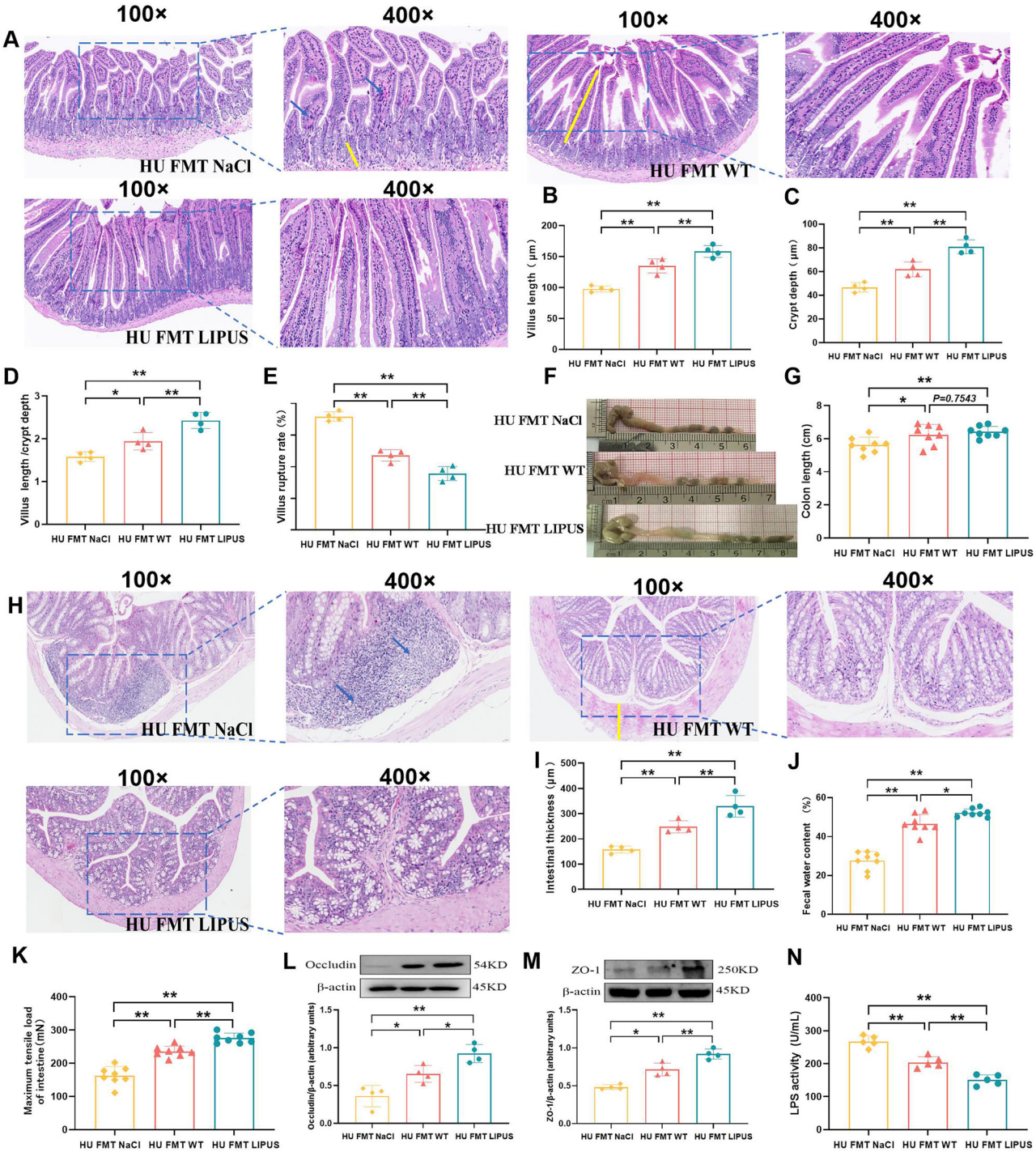

Fig. 9 | The effect of fecal microbiota transplantation from abdominal LIPUS treated mice on intestinal barrier and function in hindlimb unloaded mice. A HE staining of small intestinal tissue. **B** Villus length. **C** Crypt depth. **D** Villus length/Crypt depth. **E** Villus rupture rate. **F** Representative images of the colon of mice. **G** Colon length. **H** HE staining of colonic tissues. **I** Thickness of colonic muscle layer. **J** Fecal water content. **K** Maximum tensile load of intestine. **L** The protein level of Occludin in colon. **M** The protein level of ZO-1 in colon. **N** LPS activity. The data were expressed as mean ± SD, $^{*}P < 0.05$ and $^{**}P < 0.01$.

microenvironment. This disruption can impair gut homeostasis and elevate the risk of opportunistic pathogen colonization[32]. studies have shown that following space missions, rats exhibited shortened intestinal villi and decreased mucin production by intestinal epithelial cells[33]. Comparable findings were also observed in mice subjected to hind limb unloading for 30 days, demonstrating reduced intestinal villi, crypt depth, and muscle layer thickness, along with increased intestinal wall permeability and detrimental effects on overall health[34]. The intestinal barrier function is intimately linked to alterations in cell paracellular permeability and the functionality of tight junctions (TJs)[35]. Various proteins are instrumental in the formation of tight junctions, including Occludin, Claudin proteins, ZO proteins, and junctional adhesion molecule (JAM)[36]. A study has demonstrated that the expression of Occludin and ZO-1 decreases under simulated microgravity conditions[37]. Additionally, during spaceflight, astronauts exhibited decreased expression and altered distribution of TJ proteins such as claudin-1, claudin-4, and JAM-A, while the expression of claudin-2 increased[38]. In our study, mice in the hindlimb unloading (HU) group displayed an incomplete intestinal structure characterized by shortened

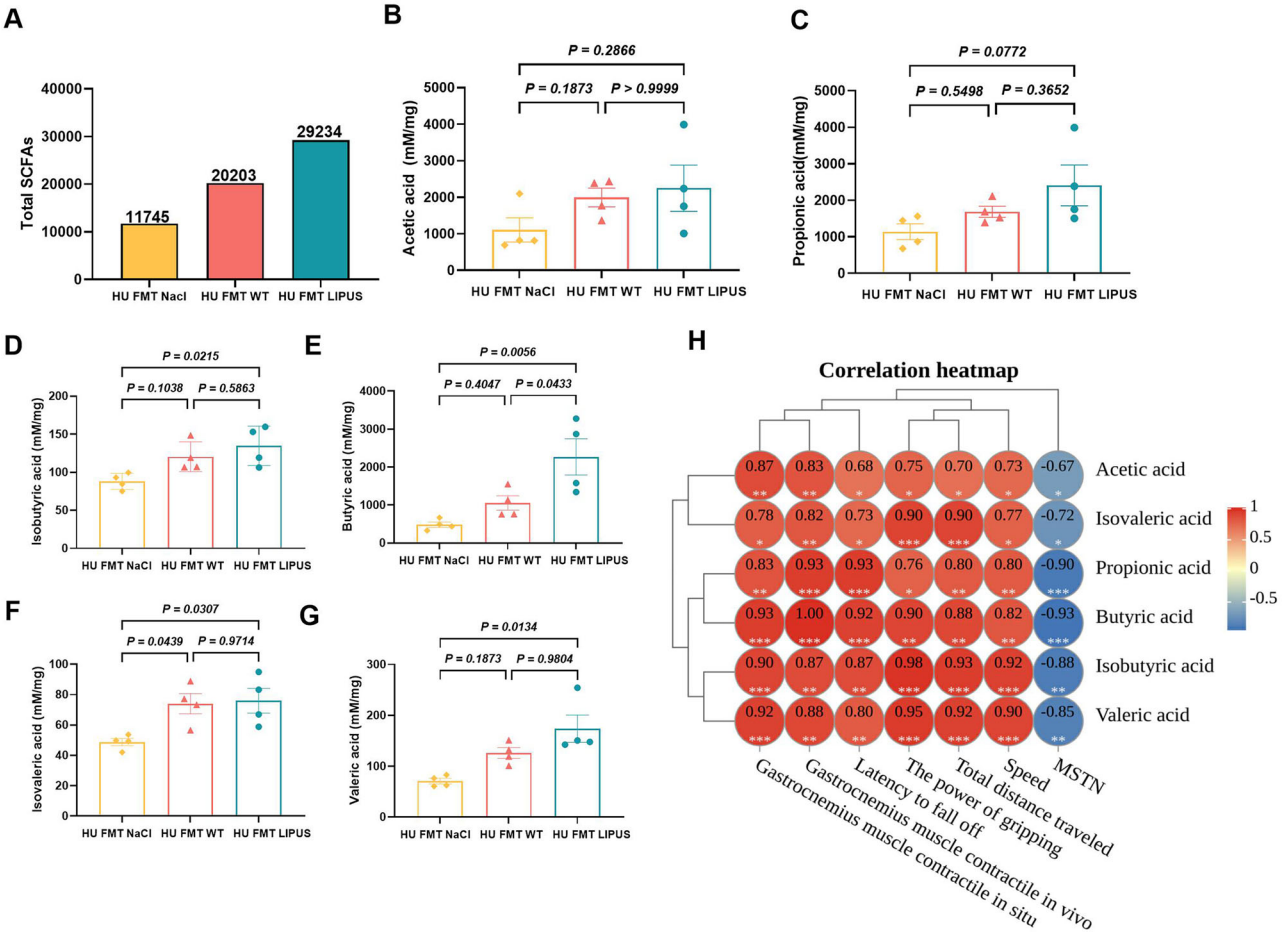

Fig. 10 | The effect of fecal microbiota transplantation from abdominal LIPUS treated mice on SCFAs in hindlimb unloaded mice. A Total SCFAs. **B** Acetic acid. **C** Propionic acid. **D** Isobutyric acid. **E** Butyric acid. **F** Isovaleric acid. **G** Valeric acid. **H** Correlation analysis between SCFAs and skeletal muscle functional indicators ($n = 4$). The data were expressed as mean ± SD, $^{*}p < 0.05$ and $^{**}p < 0.01$.

intestinal villi, shallower crypts, and thinner muscle layers. Similarly, damage to the intestinal barrier was evident, accompanied by decreased expression of tight junction proteins (Occludin and ZO-1). Furthermore, there was a notable reduction in the maximum tensile load of the intestine and an increase in fecal water content, indicating impaired intestinal function. Notably, after 28 days of abdominal low-intensity pulsed ultrasound (LIPUS) treatment, the structure and function of the intestine, as well as the integrity of the barrier, were alleviated. Lipopolysaccharide (LPS), also known as endotoxin, is a substance present in Gram-negative bacteria[39]. LPS is known to exert a pro-inflammatory effect. Increased intestinal permeability allows LPS to enter the systemic circulation, where it can activate inflammatory pathways[40]. Studies have reported that simulated microgravity can result in a transient elevation of circulating LPS levels, subsequently activating the innate immune system[41]. In our study, abdominal LIPUS was found to reduce LPS activity, thereby ensuring the integrity of the intestinal wall and preventing intestinal leakage.

Microgravity has been identified as a factor influencing the quality of skeletal muscles. Studies conducted on astronauts who have spent six months in orbit have revealed a decrease in calf muscle mass, ranging from 10% to 15%. Furthermore, transitions from slow to fast fiber types have been observed in the gastrocnemius and soleus muscles, accompanied by a significant reduction in muscle volume and mass even during shorter spaceflights[42,43]. Analogously, a two-week period of unloading in rats led to a 50% decrease in soleus muscle mass and a 17% conversion of slow to fast fibers[44]. Elevated levels of serum creatine kinase (CK) and lactate dehydrogenase (LDH) serve as indicators of muscle injury and temporary decline in muscle function. Our research findings demonstrate that, following 28 days of hindlimb unloading in mice, a reduction in gastrocnemius muscle weight and mass was evident. Concurrently, there was a marked increase in CK and LDH levels, suggesting that microgravity may contribute to muscle damage and functional impairment. However, abdominal ultrasound treatment resulted in an increase in muscle weight and mass, as well as enhanced exercise capacity. MSTN, a well-documented inhibitory factor in muscle growth, can lead to muscle atrophy when overexpressed[45]. AKT, positioned downstream of MSTN, and its principal downstream molecule, mTOR, regulate protein synthesis[46,47]. Abdominal ultrasound was found to suppress MSTN, activate the AKT/mTOR pathway, and alleviate muscle atrophy induced by hindlimb unloading. Notably, transplanting fecal microbiota from mice treated with abdominal ultrasound produced consistent results. In summary, abdominal ultrasound prevents muscle atrophy caused by hindlimb unloading through the regulation of gut microbiota disorders.

The metabolic byproducts of gut microbiota, specifically short-chain fatty acids (SCFAs), exert regulatory effects on skeletal muscle within the body. The primary SCFAs include acetic acid, propionic acid, and butyric acid. Butyric acid serves as the primary energy source for colonocytes, possesses anti-inflammatory properties, and is a crucial metabolite for maintaining intestinal environment stability and strengthening intestinal barrier function[48–50]. Studies have indicated that the main species responsible for SCFAs production are *Helicobacter pylori*, *lactic acid bacteria*, and *rumen bacteria*, with contributions from certain fungal species in smaller quantities[51]. Oral administration of butyrate has been shown to increase

skeletal muscle mass and ameliorate muscle atrophy in aged mice[52]. Notably, there is a strong correlation between alterations in gut microbiota, SCFAs levels, and intestinal injury. Intestinal injury can lead to reduced SCFAs production, whereas the intake of probiotics or dietary fiber can enhance SCFAs levels[53–55]. Research has demonstrated that butyrate can mitigate skeletal muscle atrophy in diabetic nephropathy by bolstering intestinal barrier function and activating FFA2-mediated PI3K/AKT/mTOR signaling[56]. Our results revealed that mice subjected to hindlimb unloading for 28 days exhibited a significant reduction in SCFAs levels, primarily influenced by alterations in the populations of *Bacteroides*, *Parabacteroides*, and *Alloprevotella*. *Parabacteroides* exhibits physiological characteristics associated with carbohydrate metabolism and SCFAs secretion[57], and studies have shown that Parabacteroides and its metabolite pentadecanoic acid have a protective effect on mice with non-alcoholic fatty liver disease by restoring intestinal barrier function and reducing the expression of serum lipopolysaccharides and liver pro-inflammatory cytokines[58]. Therefore, *Parabacteroides* plays a crucial role in maintaining intestinal barrier integrity. *Alloprevotella* is considered a beneficial bacterium capable of producing butyric acid[59]. Research has indicated that berberine can influence blood glucose levels by regulating the gut microbiota structure, leading to an increased abundance of *Alloprevotella*[60]. Additionally, Alloprevotella has been shown to possess anti-inflammatory properties[61]. After abdominal low-intensity pulsed ultrasound (LIPUS) treatment, SCFAs levels increased, skeletal muscle atrophy was alleviated, and muscle fiber area, grip strength, and exercise capacity were improved. Abdominal LIPUS altered the gut microbiota composition and SCFAs levels, which in turn mitigated skeletal muscle atrophy. Pearson correlation analysis showed that SCFAs content after abdominal LIPUS was positively correlated with skeletal muscle functional indicators and negatively correlated with MSTN. Therefore, SCFAs serve as intermediate mediators in the abdominal ultrasound therapy process.

In summary, the application of low-intensity pulse ultrasound (LIPUS) to the abdomen has been demonstrated to effectively counteract the disruption of gut microbiota, facilitate the restoration of intestinal damage, and subsequently prevent skeletal muscle loss in mice subjected to hind limb unloading. Thus, abdominal LIPUS emerges as a promising intervention to mitigate gut microbiota dysfunction and skeletal muscle atrophy in astronauts or patients confined to long-term bed rest.

It is important to acknowledge that this study is subject to a notable limitation. Specifically, while the study has shown that abdominal LIPUS stimulation can prevent skeletal muscle atrophy in mice caused by hind limb unloading by improving disrupted gut microbiota balance, it has not yet identified the most responsive individual bacterium to LIPUS nor validated its therapeutic effects. Therefore, further research is required to elucidate the mechanism through which abdominal LIPUS stimulation enhances the intestinal microenvironment and regulates systemic skeletal muscle atrophy, thereby providing more definitive evidence for its potential clinical application.

Methods

Animals

Fifty-six male C57BL/6 mice (6 weeks old, 22 ± 3 g) were provided by the Animal Experimental Breeding Research Center of Shaanxi Normal University (Xi'an, China). These mice were housed under controlled environmental conditions, including a standard room temperature of 22 °C, a humidity range of 55–60%, and a regulated 12-h light/dark cycle. They had unrestricted access to food and water throughout the study period. All experimental procedures involving animals adhered rigorously to the National Institutes of Health Guide for the Care and Use of Laboratory Animals, and were granted approval by the Experimental Animal Ethics Committee of Shaanxi Normal University.

Grouping and intervention methods

Mice were divided into three groups: normal control (NC, $n = 8$), hindlimb unloading (HU, $n = 8$), and hindlimb unloading with abdominal LIPUS intervention (HU + LIPUS, $n = 8$). In the HU group, mice were subjected to hindlimb unloading by tail suspension, with their bodies maintained at a 30° angle to the ground while their forelimbs remained free to move along the cage floor. Throughout the experimental period, all mice had unrestricted access to food and water[62]. Mice in the NC group were individually housed in cages identical to those used for the HU mice but without hindlimb unloading. Mice in the HU + LIPUS group underwent LIPUS treatment on their shaved abdomen while suspended, for 20 min per day over a span of 28 days (Fig. 1A). A 1.8-cm-diameter ultrasonic probe was employed for this purpose. The LIPUS device, supplied by the Intelligent Medical Ultrasound Lab at Fudan University (Shanghai, China), generated 200-μs bursts of 1.5-MHz acoustic sine waves, repeated at a frequency of 1.0 kHz, with an intensity (ISATA) of 30 mW/cm². The intensity was precisely calibrated using a high-resolution ultrasound power meter (UPM-DT-1000PA, Ohmic Instruments, MO, USA) with a 1 mW resolution. Mice in the HU group underwent a sham procedure using an ineffective probe placed at the same location.

Additionally, fecal microbiota transplantation (FMT) was utilized to confirm the role of gut microbiota in mediating the protective effects of LIPUS against muscle atrophy induced by microgravity. The hindlimb unloaded mice were further divided into three subgroups: the hindlimb unloading with fecal microbiota transplantation from sodium chloride-treated mice group (HU FMT NaCl), the hindlimb unloading with fecal microbiota transplantation from wild-type mice group (HU FMT WT), and the hindlimb unloading with fecal microbiota transplantation from mice undergoing abdominal LIPUS treatment group (HU FMT LIPUS) (Fig. 7A). Following the final gavage administration one day prior to euthanasia, the mice were fasted for 12 h. Subsequently, fecal samples were collected and stored at −80 °C. At the conclusion of the entire experimental period, the mice were weighed and euthanized, and samples of serum, skeletal muscle, small intestine, and colon tissues were harvested from all groups for comprehensive analysis. On the day preceding formal tissue collection, mice were anesthetized via intraperitoneal injection of sodium pentobarbital (30–50 mg/kg, dosed precisely by body weight) to obtain baseline data for in vivo gastrocnemius muscle contractile function. On the day of collection, anesthesia was re-administered via intraperitoneal injection within the same dosage range (adjusted based on real-time body weight) to perform in situ gastrocnemius muscle contraction force measurements, ensuring experimental data accuracy. Following in vitro experiments, euthanasia was administered via intraperitoneal injection of the anesthetic at 60–100 mg/kg. All procedures were performed by trained personnel in accordance with standardized protocols to minimize suffering.

Hematoxylin and eosin (HE) staining

The skeletal muscle tissue was extracted from the fixation solution, undergoing dehydration through a series of graded alcohol solutions before being embedded in paraffin. Using a semi-automatic slicing machine (Dako, Tokyo, Japan), a paraffin section with a thickness ranging from 8 to 10 micrometers was prepared. The section was then dewaxed and stained with hematoxylin and eosin. Images of the stained sections were captured at a magnification of 200× using an inverted microscope (Olympus BX-51, Japan). Subsequently, the average cross-sectional area of muscle fibers was measured using ImageJ. Each group consists of 4 sections, with 3 random fields of view averaged per section.

The duodenum was excised, thoroughly rinsed with normal saline, and subsequently fixed in a 4% tissue fixative. It was then processed through dehydration and embedding procedures to produce sections with a thickness of 6 μm. These sections were stained with hematoxylin-eosin (HE). The intestinal morphology was examined and photographed at magnifications of 100× and 400× using an inverted microscope (Olympus BX-51, Japan). Various intestinal parameters were measured using ImageJ, including villus length, crypt depth, the villus-to-crypt ratio (villus length divided by crypt depth), villus rupture rate, and intestinal wall thickness. The measurements were conducted as follows: villi length was determined from the tip of the villus to the villus-crypt junction; crypt depth was measured from the crypt

opening to its base; and intestinal wall thickness was assessed from the outer surface of the intestine to the junction of the submucosa and muscular layer, encompassing both the serosa layer and the muscular layer[63]. Each group consists of 4 sections from 4 mice, with 3 random fields of view averaged per section. Villi rupture rate were quantified through full-section scanning.

Grip strength test

Grip strength was evaluated for all four limbs of the mice using a grip strength meter (model YLS13A, manufactured by Anhui Zheng Hua Bioinstrumentation Co., Ltd., located in Huaibei, Anhui, China). Each mouse underwent three consecutive tests without rest in between. For each mouse, the average of the three peak grip strengths recorded was calculated.

Rotarod performance test

After undergoing a four-week period of tail suspension, the mice participated in a single exhaustive training session and were subsequently evaluated using a rotating rod apparatus (KW-6C, Nanjing, China). The initial speed was set at 35 revolutions per minute (rpm), with an acceleration period lasting 280 s, which also served as the total duration of the test. Upon completion of this phase, the speed was incremented by 40 rpm, and thereafter remained constant. The maximum duration that the mice were able to maintain their balance and walk on the accelerating rotating rod was recorded, serving as an indicator of their exercise endurance capacity.

Gastrocnemius muscle contraction in vivo and in situ test and maximum tensile load of intestine

The gastrocnemius muscle contraction was evaluated both in vivo and in situ using a muscle testing system instrument (model 1305A, Aurora, ON, Canada). For the in vivo test, the fur on the hindlimbs was shaved, and the mice were positioned supine on the testing platform. The head was stabilized, and the mouse's foot was secured on the opposite side of the platform to prevent movement due to muscle contraction during electrical stimulation. Two metal electrodes were placed on the sural nerve innervating the gastrocnemius muscle to ensure effective electrical stimulation. The instrument executed the testing protocol, delivering 100 Hz electrical stimulation to the gastrocnemius muscle via the electrodes, thereby eliciting muscle contraction. Each mouse underwent three repeated tests, and the obtained values were statistically analyzed.

The in situ test method for gastrocnemius muscle contraction follows a similar procedure. Surgical sutures are used to secure the distal end of the gastrocnemius muscle, and a lamp is utilized to maintain the experimental temperature at 37 °C. Two metal electrodes are positioned on the sural nerve innervating the gastrocnemius muscle to guarantee effective electrical stimulation. The testing instrument then executes the predefined program, delivering 100 Hz electrical stimulation to the gastrocnemius muscle through the electrodes, thus inducing muscle contraction. Each mouse undergoes three repetitions of the test, and the resulting values are subjected to statistical analysis.

A 2-cm segment of small intestine was excised from the pylorus of the stomach and positioned in a groove. Krebs-Ringer solution was added to maintain the physiological environment, and a light source was used to keep the experimental temperature at 37 °C. A muscle testing system was employed to gradually stretch the intestine until it ruptured, allowing for the determination of the maximum tensile load.

Fecal water content

Following a period of 28 days of modeling, the feces should be collected between 9 am and 11 am prior to execution. The water content of the feces is determined by comparing its wet weight to its dry weight. Initially, the wet weight of the feces is measured. Subsequently, the feces are placed in a drying oven set at 60°C for 30min. Following this drying process, the weight is recorded as the dry weight. The moisture content of the feces is then calculated using a specific formula.

$$\text{Fecal water content}(\%) = \text{wet weight} - \text{dry weight}/\text{wet weight} \times 100\%$$

Fecal microbial transplantation

Prior to fecal microbiota transplantation (FMT), recipient mice underwent daily gastric lavage with a solution containing a cocktail of three antibiotics: 1.25mg/L Vancomycin, 2.5mg/L Ampicillin, and 2.5mg/L Metronidazole for a duration of one week. Additionally, Ampicillin was supplemented in the drinking water of these mice at a concentration of 1 g/L. The donor mice were stratified into two groups: an abdominal LIPUS treatment group ($n = 4$, undergoing abdominal LIPUS treatment for 28 days) and a wild-type (WT) control group ($n = 4$, receiving sham abdominal LIPUS treatment). The overall preparation of donor fecal transplant materials adhered to previously established experimental protocols with similar assays. Fresh fecal samples were collected from donor mice in both the LIPUS and WT groups. These samples were homogenized with sterile phosphate-buffered saline (PBS) and subsequently filtered through a 20 μm filter to eliminate impurities. The filtrate was then centrifuged at 12,000 rpm for 15 min at 4 °C to separate microorganisms and other particulate matter. The isolated filtrate was diluted with PBS to a concentration of 400 mg/mL (400 mg original fecal weight per mL of PBS) and then administered by oral gavage to hindlimb unloaded mice every other day. Each mouse received 0.2 mL of the solution, with the treatment continuing for four weeks[64].

DNA extraction of intestinal contents and 16S rRNA high throughput sequencing

The soil and feces genomic DNA extraction kit (DP712) from Tiangen (China) was employed to isolate DNA from feces. Subsequently, 1% agarose gel electrophoresis was conducted to ascertain the purity and concentration of the extracted DNA. An appropriate aliquot of the sample was transferred to a centrifuge tube and diluted with sterile water to achieve a concentration of 1 ng/μL. Two highly variable regions of the bacterial 16S rRNA gene, V3-V4, were amplified using primers 341F (CCTAYGGRBGCACAG) and 806R (GGACTACHVGGTWTTCTAAT). Sequencing libraries were constructed using the NEB Next®Ultra™ DNA Library Prep Kit for Illumina (NEB, USA), following the manufacturer's instructions, and index codes were incorporated. The quality of the libraries was evaluated using the Qubit@ 2.0 Fluorometer (Thermo Scientific) and the Agilent Bioanalyzer 2100 system. Ultimately, the library was sequenced on an Illumina Miseq/HiSeq2500 platform, generating 250 bp/300 bp paired-end reads.

Bioinformatics analysis primarily entailed the utilization of the QIIME2 dada2 plugin for quality control of the sequencing results. This included tasks such as trimming, denoising, and concatenating the reads, culminating in the acquisition of feature sequence tables after the removal of chimeric sequences. Subsequently, the representative sequences of Amplicon Sequence Variants (ASVs) were compared against the pre-trained GREENGENES database to produce a taxonomic classification table at the species level.

To detect alterations in gut microbiota abundance between groups and samples, statistical analyses were performed using ANOVA and Kruskal–Wallis methods. α Diversity indices at the feature sequence level, comprising observed Operational Taxonomic Units (OTUs), Chao1, and Shannon, were employed to assess sample diversity.

Short chain fatty acid (SCFA) analysis

SCFAs were analyzed using a GC-MS single quadrupole instrument (QP-2010Ultra, Shimadzu). Specifically, 0.1 g of mouse feces were weighed and placed in 1 milliliter of a 0.5% aqueous phosphoric acid solution. The mixture was vortexed, thoroughly mixed, and centrifuged to obtain the supernatant. This supernatant was then transferred to a solution of ethyl acetate, mixed well, and centrifuged again to obtain the supernatant intended for testing.

For the GC-MS analysis, an unsplit injection of 1 microliter of the sample was performed at 200 °C. The initial column temperature was maintained at 35 °C for 5 min, after which it was increased to 120 °C at a rate of 15 °C/min. Subsequently, the temperature was raised to 170 °C at a rate of 5 °C/min and then further increased to 250 °C at a rate of 20 °C/min, where

it was held for an additional 2 min (total run time: 30 min). The resulting data were subjected to statistical analysis.

Western blot analysis

A quantity of 0.05 g of gastrocnemius muscle tissue was weighed and homogenized using 500 μL of RIPA lysate. Subsequently, the protein concentration within the gastrocnemius muscle was assessed utilizing the BCA Protein Analysis Kit sourced from zhhcbio, Inc. (Xian, China). For electrophoresis, an SDS-polyacrylamide gel with a concentration range of 8–12% was employed, and the proteins were then transferred onto a nitrocellulose membrane.

Immunoblotting was conducted with primary antibodies being incubated overnight at 4 °C. Following this, the membrane was incubated with the appropriate secondary antibodies (provided by zhuangzhibio, Inc., Xian, China) for a duration of 1 h at room temperature. Immunoreactive proteins were visualized using enhanced chemiluminescence (ECL) technology from Emerson. The Azure Biosystems C300 imaging system, located in California, USA, was utilized to capture the protein bands.

The specific antibodies used in this study included MSTN (DF13273) and ActRIIB (DF9146) from Affinity, Akt (CST 9272s) and mTOR (CST 2972s) from Cell Signaling Technology, Occludin (D291080) from Sangon Biotech, and ZO-1 (A11417) from ABclonal. Additionally, GAPDH (GB11002) and β-Actin (GB11001) were sourced from Servicebio. The grayscale values of the bands were analyzed using Image J software.

Serum analysis

Biochemical reagent kits, sourced from Nanjing Jiancheng College of Biotechnology (Nanjing, China) for creatine kinase (CK) and lactate dehydrogenase (LDH), and from Beijing Solaibao Technology Co., Ltd. (China) for lipopolysaccharide (LPS), were utilized to determine their respective activities in mouse serum. The testing procedure, including all specific steps, was meticulously followed in accordance with the manufacturer's instructions provided with each reagent kit. Absorbance readings were obtained using a Model 680 microplate reader manufactured by Bio-Rad Corp (Philadelphia, PA, USA).

Statistical analysis

All analyses were conducted using GraphPad Prism version 9.4 (GraphPad Software). The data are presented as the mean ± standard deviation. The normality of the data was verified using the Normality and Lognormality tests. If the data followed a normal distribution, the difference between variables was assessed using one-way analysis of variance (ANOVA) with Tukey's multiple comparisons test. Conversely, if the data did not meet the criteria for normality, the Kruskal–Wallis test was employed to evaluate differences. Pearson's correlation coefficient was utilized to investigate potential correlations between microbial communities and skeletal muscle function. Statistical significance was set at a P value of <0.05.

Data availability

16S sequencing and RNA-seq data have been deposited at https://doi.org/10.6084/m9.figshare.28107353.v1. Any additional information required to reanalyze the data reported in this paper is available from the corresponding author.

Received: 25 February 2025; Accepted: 26 July 2025;
Published online: 27 October 2025

References

1. Jollet, M. et al. Does physical inactivity induce significant changes in human gut microbiota? New answers using the dry immersion hypoactivity model. *Nutrients* **13**, 3865 (2021).
2. Kirkpatrick, A. W. et al. Do we have the guts to go? The abdominal compartment, intra-abdominal hypertension, the human microbiome and exploration class space missions. *Can. J. Surg.* **63**, E581–E593 (2020).
3. Chen, K. Z. M., Vu, L. M. & Vollmer, A. C. Cultivation in long-term simulated microgravity is detrimental to pyocyanin production and subsequent biofilm formation ability of Pseudomonas aeruginosa. *Microbiol. Spectr.* **12**, e00211-24 (2024).
4. White, R. J. & Averner, M. Humans in space. *Nature* **409**, 1115–1118 (2001).
5. Juhl, O. J. et al. Update on the effects of microgravity on the musculoskeletal system. *npj Microgravity* **7**, 1–15 (2021).
6. Harrison, B. C. et al. Skeletal muscle adaptations to microgravity exposure in the mouse. *J. Appl. Physiol.* **95**, 2462–2470 (2003).
7. Mancin, L., Wu, G. D. & Paoli, A. Gut microbiota–bile acid–skeletal muscle axis. *Trends Microbiol.* **31**, 254–269 (2023).
8. Giron, M., Thomas, M., Dardevet, D., Chassard, C. & Savary-Auzeloux, I. Gut microbes and muscle function: can probiotics make our muscles stronger?. *J. Cachexia. Sarcopenia Muscle* **13**, 1460–1476 (2022).
9. Fang, W.-Y. et al. Triptolide prevents LPS-induced skeletal muscle atrophy via inhibiting NF-κB/TNF-α and regulating protein synthesis/degradation pathway. *Br. J. Pharmacol.* **178**, 2998–3016 (2021).
10. Tan, W. et al. Phosphatidylcholine ameliorates lps-induced systemic inflammation and cognitive impairments via mediating the gut–brain axis balance. *J. Agric. Food Chem.* **68**, 14884–14895 (2020).
11. Lahiri, S. et al. The gut microbiota influences skeletal muscle mass and function in mice. *Sci. Transl. Med.* **11**, eaan5662 (2019).
12. Okamoto, T. et al. Microbiome potentiates endurance exercise through intestinal acetate production. *Am. J. Physiol. Endocrinol. Metab.* **316**, E956–E966 (2019).
13. Nay, K. et al. Gut bacteria are critical for optimal muscle function: a potential link with glucose homeostasis. *Am. J. Physiol. Endocrinol. Metab.* **317**, E158–E171 (2019).
14. Qiu, Y. et al. Depletion of gut microbiota induces skeletal muscle atrophy by FXR-FGF15/19 signalling. *Ann. Med.* **53**, 508–522 (2021).
15. Montalti, C. S. et al. Effects of low-intensity pulsed ultrasound on injured skeletal muscle. *Braz. J. Phys. Ther.* **17**, 343–350 (2013).
16. Song, W.-S. et al. Neuroprotection by Abdominal Ultrasound in Lipopolysaccharide-Induced Systemic Inflammation. *Int. J. Mol. Sci.* **24**, 9329 (2023).
17. Yang, F.-Y., Chan, W.-H., Gao, C.-Y., Zheng, Y.-T. & Ke, C.-H. Transabdominal ultrasound alleviates LPS-induced neuroinflammation by modulation of TLR4/NF-κB signaling and tight junction protein expression. *Life Sci.* **325**, 121769 (2023).
18. Garrett-Bakelman, F. E. et al. The NASA Twins Study: a multidimensional analysis of a year-long human spaceflight. *Science* **364**, eaau8650 (2019).
19. Siddiqui, R. & Khan, N. A. Microbiome and one health: potential of novel metabolites from the gut microbiome of unique species for human health. *Microorganisms* **11**, 481 (2023).
20. Bonanni, R., Cariati, I., Marini, M., Tarantino, U. & Tancredi, V. Microgravity and musculoskeletal health: what strategies should be used for a great challenge?. *Life* **13**, 1423 (2023).
21. Marullo, A. L. & O'Halloran, K. D. Microbes, metabolites and muscle: Is the gut–muscle axis a plausible therapeutic target in Duchenne muscular dystrophy?. *Exp. Physiol.* **108**, 1132–1143 (2023).
22. Huang, B., Li, D.-G., Huang, Y. & Liu, C.-T. Effects of spaceflight and simulated microgravity on microbial growth and secondary metabolism. *Mil. Med. Res.* **5**, 18 (2018).
23. Voorhies, A. A. et al. Study of the impact of long-duration space missions at the International Space Station on the astronaut microbiome. *Sci. Rep.* **9**, 9911 (2019).
24. Jiang, P., Green, S. J., Chlipala, G. E., Turek, F. W. & Vitaterna, M. H. Reproducible changes in the gut microbiome suggest a shift in microbial and host metabolism during spaceflight. *Microbiome* **7**, 113 (2019).
25. Ritchie, L. E. et al. Space environmental factor impacts upon murine colon microbiota and mucosal homeostasis. *PLoS One* **10**, e0125792 (2015).

26. Siddiqui, R., Akbar, N. & Khan, N. A. Gut microbiome and human health under the space environment. *J. Appl. Microbiol.* **130**, 14–24 (2021).
27. Bharindwal, S., Goswami, N., Jha, P., Pandey, S. & Jobby, R. Prospective use of probiotics to maintain astronaut health during spaceflight. *Life* **13**, 727 (2023).
28. Sun, H. et al. Gut commensal Parabacteroides distasonis alleviates inflammatory arthritis. *Gut* **72**, 1664–1677 (2023).
29. Ulger Toprak, N. et al. Alloprevotella rava isolated from a mixed infection of an elderly patient with chronic mandibular osteomyelitis mimicking oral squamous cell carcinoma. *N. Microbes N. Infect.* **42**, 100880 (2021).
30. Zhang, L. et al. The oral microbiota may have influence on oral cancer. *Front. Cell. Infect. Microbiol.* **9**, 476 (2020).
31. Dai, D. et al. Organic acids as alternatives for antibiotic growth promoters alter the intestinal structure and microbiota and improve the growth performance in broilers. *Front. Microbiol.* **11**, 618144 (2021).
32. Li, P. et al. Simulated microgravity disrupts intestinal homeostasis and increases colitis susceptibility. *FASEB J.* **29**, 3263–3273 (2015).
33. Shi, J. et al. Intestinal microbiota contributes to colonic epithelial changes in simulated microgravity mouse model. *FASEB J.* **31**, 3695–3709 (2017).
34. Lagereva, E., Mashkin, M. & Andreev-Andrievskiy, A. Morphological and functional changes in the murine intestine during 30-day Hindlimb unloading and recovery. *Front. Physiol.* **12**, 139–148 (2021).
35. Horowitz, A., Chanez-Paredes, S. D., Haest, X. & Turner, J. R. Paracellular permeability and tight junction regulation in gut health and disease. *Nat. Rev. Gastroenterol. Hepatol.* **20**, 417–432 (2023).
36. Nehme, Z., Roehlen, N., Dhawan, P. & Baumert, T. F. Tight junction protein signaling and cancer biology. *Cells* **12**, 243 (2023).
37. Alvarez, R. et al. A simulated microgravity environment causes a sustained defect in epithelial barrier function. *Sci. Rep.* **9**, 17531 (2019).
38. Blair, S. A., Kane, S. V., Clayburgh, D. R. & Turner, J. R. Epithelial myosin light chain kinase expression and activity are upregulated in inflammatory bowel disease. *Lab. Invest.* **86**, 191–201 (2006).
39. Izadparast, F., Riahi-Zajani, B., Yarmohammadi, F., Hayes, A. W. & Karimi, G. Protective effect of berberine against LPS-induced injury in the intestine: a review. *Cell Cycle* **21**, 2365–2378 (2022).
40. Verhaar, B. J. H. et al. Gut microbiota in hypertension and atherosclerosis: a review. *Nutrients* **12**, 2982 (2020).
41. Yang, Y. et al. Estrogen inhibits the overgrowth of Escherichia coli in the rat intestine under simulated microgravity. *Mol. Med. Rep.* **17**, 2313–2320 (2018).
42. Bettis, T., Kim, B.-J. & Hamrick, M. W. Impact of muscle atrophy on bone metabolism and bone strength: implications for muscle-bone crosstalk with aging and disuse. *Osteoporos. Int.* **29**, 1713–1720 (2018).
43. Zhang, J. et al. Identification of the optimal dose and calpain system regulation of tetramethylpyrazine on the prevention of skeletal muscle atrophy in hindlimb unloading rats. *Biomed. Pharmacother.* **96**, 513–523 (2017).
44. Gopalakrishnan, R. et al. Muscle volume, strength, endurance, and exercise loads during 6-month missions in space. *Aviat. Space Environ. Med.* **81**, 91–102 (2010).
45. Lee, S. J. Myostatin: a skeletal muscle chalone. *Annu. Rev. Physiol.* **85**, 269–291 (2023).
46. Léger, B. et al. Akt signalling through GSK-3beta, mTOR and Foxo1 is involved in human skeletal muscle hypertrophy and atrophy. *J. Physiol.* **576**, 923–933 (2006).
47. Hanson, A. M. et al. Inhibiting myostatin signaling partially mitigates structural and functional adaptations to hindlimb suspension in mice. *npj Microgravity* **9**, 2 (2023).
48. Kim, M. H., Kang, S. G., Park, J. H., Yanagisawa, M. & Kim, C. H. Short-chain fatty acids activate GPR41 and GPR43 on intestinal epithelial cells to promote inflammatory responses in mice. *Gastroenterology* **145**, 396–406.e1-10 (2013).
49. Frampton, J., Murphy, K. G., Frost, G. & Chambers, E. S. Short-chain fatty acids as potential regulators of skeletal muscle metabolism and function. *Nat. Metab.* **2**, 840–848 (2020).
50. Donohoe, D. R. et al. The microbiome and butyrate regulate energy metabolism and autophagy in the mammalian colon. *Cell Metab.* **13**, 517–526 (2011).
51. Vacca, M. et al. The controversial role of human gut lachnospiraceae. *Microorganisms* **8**, 573 (2020).
52. Mikelsaar, M. & Mändar, R. Commentary: gut microbiome and space travelers' health: state of the art and possible pro/prebiotic strategies for long-term space missions. *Front. Physiol.* **12**, 651977 (2021).
53. Jollet, M. et al. Does simulated microgravity induce significant changes in human gut microbiota? New answers with dry immersion, an innovative ground-based model. *Res. Sq.* https://doi.org/10.21203/rs.3.rs-52630/v1 (2020).
54. Purdy, R. E. et al. Effect of simulated microgravity on vascular contractility. *J. Appl. Physiol.* **85**, 1307–1315 (1998).
55. Li, Y. et al. Review: effect of gut microbiota and its metabolite SCFAs on radiation-induced intestinal injury. *Front. Cell Infect. Microbiol.* **11**, 577236 (2021).
56. Tang, G. et al. Butyrate ameliorates skeletal muscle atrophy in diabetic nephropathy by enhancing gut barrier function and FFA2-mediated PI3K/Akt/mTOR signals. *Br. J. Pharm.* **179**, 159–178 (2022).
57. Cui, Y. et al. Roles of intestinal Parabacteroides in human health and diseases. *FEMS Microbiol. Lett.* **369**, fnac072 (2022).
58. Wei, W. et al. Parabacteroides distasonis uses dietary inulin to suppress NASH via its metabolite pentadecanoic acid. *Nat. Microbiol.* **8**, 1534–1548 (2023).
59. Ma, Q. et al. Investigation of gut microbiome changes in type 1 diabetic mellitus rats based on high-throughput sequencing. *Biomed. Pharmacother.* **124**, 109873 (2020).
60. Yang, S., Li, D., Yu, Z., Li, Y. & Wu, M. Multi-pharmacology of berberine in atherosclerosis and metabolic diseases: potential contribution of gut microbiota. *Front. Pharm.* **12**, 709629 (2021).
61. Cheng, M. et al. Integrative analysis of microbiome and metabolome in rats with Gest-Aid Plus Oral Liquid supplementation reveals mechanism of its healthcare function. *Food Qual. Saf.* **5**, fyab010 (2021).
62. Wang, J. et al. PGC-1α over-expression suppresses the skeletal muscle atrophy and myofiber-type composition during hindlimb unloading. *Biosci. Biotechnol. Biochem.* **81**, 500–513 (2017).
63. Frankel, W. L. et al. Glutamine enhancement of structure and function in transplanted small intestine in the rat. *JPEN J. Parenter. Enter. Nutr.* **17**, 47–55 (1993).
64. Hamilton, M. J., Weingarden, A. R., Sadowsky, M. J. & Khoruts, A. Standardized frozen preparation for transplantation of fecal microbiota for recurrent Clostridium difficile infection. *Am. J. Gastroenterol.* **107**, 761–767 (2012).

Acknowledgements

This work was supported by the National Natural Science Foundation of China (Nos. 12374442, 12034005, 11974233), and the Shaanxi Provincial Natural Science Foundation (No.2025JC-YBMS-046).

Author contributions

All authors participated in the design, interpretation of the studies, analysis of the data, and review of the manuscript. L.T. and L.S. designed the experiments. D.T. developed the LIPUS instrument. Y.Y. conducted most of the experiments and performed the analysis. Y.Z. and H.Z. participated in the establishment of the animal model and LIPUS treatment. X.F. and J.G. were

responsible for the calibration of LIPUS instruments. Y.Y. wrote the manuscript. All authors read and approved the final manuscript.

Competing interests
The authors declare no competing interests.

Additional information
Supplementary information The online version contains supplementary material available at https://doi.org/10.1038/s41526-025-00514-8.

Correspondence and requests for materials should be addressed to Lijun Sun, Liang Tang or Dean Ta.